

Revised by C. Lautenberger
Original chapter authored by C.L. Tien, K.Y. Lee,
and A.J. Stretton

Introduction

Thermal radiation is the dominant mode of heat transfer in flames with characteristic lengths exceeding approximately 0.2 m. It is for this reason that quantitative analysis of fire dynamics requires a working knowledge of thermal radiation. This chapter will introduce the fundamentals of thermal radiation and offer several methods for calculating radiant heat transfer in fires. Basic thermal radiation concepts are presented with an emphasis on application to fire phenomena; the reader is referred the literature for specialized topics [1–4].

Basic Concepts

The Nature of Thermal Radiation

Whereas conduction and convection require direct contact for objects at different temperatures to exchange heat, thermal radiation is a distinct mechanism of heat transfer that allows spatially separated objects at different temperatures to transfer heat. Although the Earth is separated from its Sun by 1.5×10^{11} m of near perfect

vacuum, we have all enjoyed its radiative heat transfer on cool days, and cursed it on hot ones.

All objects with a finite temperature emit thermal radiation through a physical mechanism related to electron oscillations and transitions. As an object's absolute temperature increases, these electron oscillations and transitions become more rapid, resulting in increased radiant emission. Since all objects emit radiation, all objects also have a certain amount of thermal radiation impinging upon them (originating from other emitting objects). It is the net difference between incoming and outgoing thermal radiation that leads to a net rate of radiant heat transfer between objects at different temperatures, and quantification of this rate is usually the ultimate goal of a radiation heat transfer analysis.

The nature of thermal radiation transport can be explained on the basis of quantum mechanics or electromagnetic wave theory. In the general quantum mechanical consideration, electromagnetic radiation is viewed as the propagation of an ensemble of particles (usually called photons or quanta). These particles, being generated by sub-molecular processes that are fed by an object's internal energy, carry different energies. The energy of a photon (e , J) is proportional to its frequency (ν , s^{-1}):

$$e = h\nu \quad (4.1)$$

The constant of proportionality in Equation 4.1 is Planck's constant, $h = 6.6256 \times 10^{-34}$ J · s. It is seen that the higher the frequency, the higher

Revised by C. Lautenberger (✉)
Reax Engineering Inc., 1921 University Ave., Berkeley,
CA 94704, USA

Original chapter authored by C.L. Tien, K.Y. Lee, and
A.J. Stretton

the photon energy. Thus, a radiation field is fully described when the flux of photons (or energy) is known for all points in the field for all directions and for all frequencies.

Due to its wave-particle duality, electromagnetic radiation exhibits properties of both particles and waves. Therefore, thermal radiation can also be explained as the propagation of electromagnetic waves. In this context, wavelength (λ) is related to frequency (ν) and the speed of light (c) as:

$$\lambda = \frac{c}{\nu} \tag{4.2}$$

The speed of light in a particular medium is denoted c , and in a vacuum it is denoted c_0 where $c_0 = 2.998 \times 10^8$ m/s. Wavelength has units of length, and for convenience it is usually given in microns (μm , or micrometers) where $1 \mu\text{m} = 10^{-6}$ m. Substituting Equation 4.2 into Equation 4.1 shows that a photon's energy increases as wavelength decreases:

$$e = \frac{hc}{\lambda} \tag{4.3}$$

Electromagnetic waves of practical significance have wavelengths ranging from 10^{-5} to $10^4 \mu\text{m}$. Figure 4.1 shows the electromagnetic spectrum spanning this range. *Thermal radiation* usually refers to electromagnetic waves with wavelengths between 10^{-1} and $10^2 \mu\text{m}$.

For comparison, visible light has wavelengths between 0.4 and 0.7 μm . Thermal radiation with wavelengths between 0.7 and 100 μm is *infrared* thermal radiation, whereas *ultraviolet* thermal radiation has wavelengths between 0.1 and 0.4 μm .

Example 1 Calculate the energy of photons (in a vacuum) with a wavelength of $10^{-1} \mu\text{m}$ (ultraviolet limit of thermal radiation) and $10^2 \mu\text{m}$ (infrared limit of thermal radiation).

Solution Equation 4.3 can be used to calculate photon energies. For the photon at the ultraviolet limit:

$$\begin{aligned} e &= \frac{hc_0}{\lambda} \\ &= \frac{(6.6256 \times 10^{-34} \text{ J} \cdot \text{s})(2.998 \times 10^8 \text{ m/s})}{10^{-1} \mu\text{m} \times (10^{-6} \text{ m}/\mu\text{m})} \\ &= 1.99 \times 10^{-18} \text{ J} \end{aligned}$$

And for the photon at the infrared limit:

$$\begin{aligned} e &= \frac{hc_0}{\lambda} \\ &= \frac{(6.6256 \times 10^{-34} \text{ J} \cdot \text{s})(2.998 \times 10^8 \text{ m/s})}{10^2 \mu\text{m} \times (10^{-6} \text{ m}/\mu\text{m})} \\ &= 1.99 \times 10^{-21} \text{ J} \end{aligned}$$

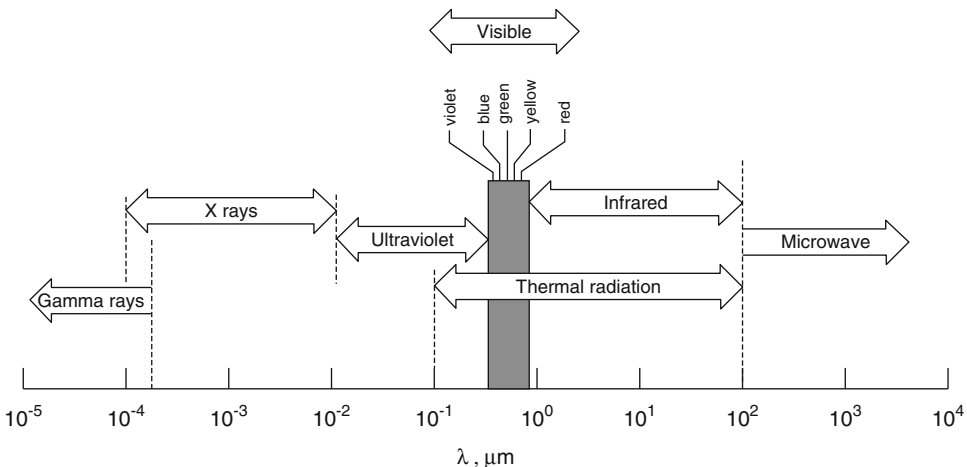


Fig. 4.1 Electromagnetic spectrum. Adapted from Incropera and DeWitt [4]

Spectral Distribution of Radiation from a Perfect Emitter

A *diffuse* surface is an idealized surface that emits thermal radiation equally in all directions, i.e. its emission exhibits no directional dependency. A *perfect emitter* is an idealized surface that emits the maximum possible thermal radiation at every wavelength. A *blackbody* is a diffuse perfect emitter that also absorbs all incident radiation.

The energy spectrum of radiation emitted by a diffuse perfect emitter, or blackbody, can be calculated from Planck's quantum theory. In particular, the spectral (or monochromatic) blackbody emissive power ($E_{\lambda,b}$, $\text{W/m}^2 \cdot \mu\text{m}$) is given by the Planck distribution:

$$E_{\lambda,b}(\lambda, T) = \frac{C_1}{\lambda^5 (\exp(C_2/\lambda T) - 1)} \quad (4.4)$$

where $C_1 = 2\pi hc_0^2 = 3.742 \times 10^8 \text{ W} \cdot \mu\text{m}^4/\text{m}^2$ is Planck's first constant (often called the first radiation constant) and $C_2 = hc_0/k = 1.439 \times 10^4 \mu\text{m} \cdot \text{K}$ is Planck's second constant

(or the second radiation constant). Note that k is the Boltzmann constant ($k = 1.3805 \times 10^{-23} \text{ J/K}$). In Equation 4.4 and throughout this chapter, a subscript "b" indicates "blackbody" and a subscript λ indicates "wavelength", e.g. $E_{\lambda,b}$ is the blackbody emissive power at a particular wavelength λ .

Spectral emissive power is plotted in Fig. 4.2 as a function of wavelength for several different blackbody temperatures. Also shown in Fig. 4.2 is a line labeled $\lambda_{\max} = C_3/T$ (where the third radiation constant is $C_3 = 2897.8 \mu\text{m} \cdot \text{K}$) that relates the wavelength corresponding to the peak spectral emissive power (λ_{\max}) to the blackbody temperature T . This is Wien's displacement law, which is obtained by differentiating Equation 4.4 with respect to T , setting that result equal to zero, and solving for λT . Wien's displacement law shows that the maximum monochromatic emissive power of a blackbody shifts to shorter wavelengths as its temperature increases. From Equation 4.3, it is also seen that the photons emitted from blackbodies high temperature (shorter wavelengths) carry more energy than photons emitted from blackbodies at lower

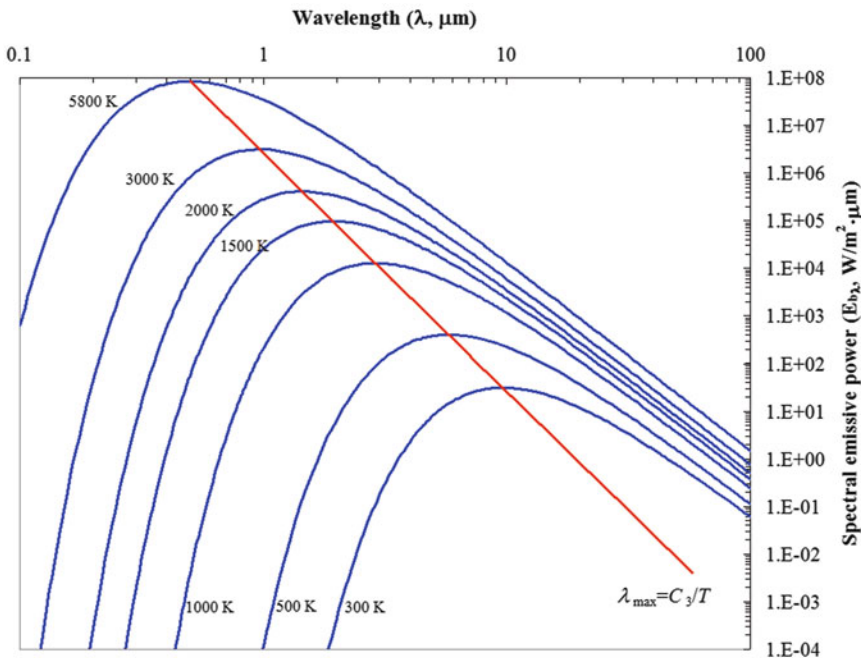


Fig. 4.2 The Planck distribution: blackbody emissive power and Wien's displacement law

temperatures (longer wavelengths), a result that one intuitively expects.

The Stefan-Boltzman Law is obtained by integrating the spectral blackbody emissive power over all wavelengths:

$$E_b = \int_0^\infty E_{\lambda,b}(\lambda)d\lambda = \int_0^\infty \frac{C_1}{\lambda^5(\exp(C_2/\lambda T) - 1)}d\lambda = \sigma T^4 \quad (4.5)$$

where σ is the Stefan-Boltzman constant ($\sigma = 5.67 \times 10^{-8} \text{ W/m}^2 \cdot \text{K}^4$) and E_b is the total (integrated over all wavelengths) blackbody emissive power. It is seen that the oft-cited “fourth power dependency” of thermal radiation on temperature is a direct consequence of integrating the Planck spectral distribution over all wavelengths.

Equations 4.4 and 4.5 can be used to calculate the fraction of a blackbody’s radiant emission in a particular wavelength band, i.e. between two wavelengths. Denote $F_{\lambda_1 \rightarrow \lambda_2}$ as the fraction of a blackbody’s radiant emission between wavelengths λ_1 and λ_2 . It is then calculated as:

$$F_{\lambda_1 \rightarrow \lambda_2} = \frac{\int_0^{\lambda_2} E_{\lambda,b}d\lambda - \int_0^{\lambda_1} E_{\lambda,b}d\lambda}{E_b} = F_{0 \rightarrow \lambda_2} - F_{0 \rightarrow \lambda_1} \quad (4.6)$$

Thus, $F_{\lambda_1 \rightarrow \lambda_2}$ can be calculated from two values of $F_{0 \rightarrow \lambda}$, which is readily tabulated from Equation 4.4 as a function of λT (Table 4.1). This then makes it possible to calculate the fraction of emission between two wavelengths.

Example 2 Consider an electrically heated surface used as a heater in a flammability test. What

Table 4.1 Blackbody radiation fractions

λT ($\mu\text{m} \cdot \text{K}$)	$F_{0 \rightarrow \lambda}$ (-)	λT ($\mu\text{m} \cdot \text{K}$)	$F_{0 \rightarrow \lambda}$ (-)
200	0.000000	6200	0.754140
400	0.000000	6400	0.769234
600	0.000000	6600	0.783199
800	0.000016	6800	0.796129
1000	0.000321	7000	0.808109
1200	0.002134	7200	0.819217
1400	0.007790	7400	0.829527
1600	0.019718	7600	0.839102
1800	0.039341	7800	0.848005
2000	0.066728	8000	0.856288
2200	0.100888	8500	0.874608
2400	0.140256	9000	0.890029
2600	0.183120	9500	0.903085
2800	0.227897	10,000	0.914199
3000	0.273232	10,500	0.923710
3200	0.318102	11,000	0.931890
3400	0.361735	11,500	0.939959
3600	0.403607	12,000	0.945098
3800	0.443382	13,000	0.955139
4000	0.480877	14,000	0.962898
4200	0.516014	15,000	0.969981
4400	0.548796	16,000	0.973814
4600	0.579820	18,000	0.980860
4800	0.607559	20,000	0.985602
5000	0.633747	25,000	0.992215
5200	0.658970	30,000	0.995340
5400	0.680360	40,000	0.997967
5600	0.701046	50,000	0.998953
5800	0.720158	75,000	0.999713
6000	0.737818	100,000	0.999905

fraction of thermal radiation does this surface emit in the visible range at temperatures of 800 and 1429 K?

Solution The visible range is from 0.4 to 0.7 μm . Thus for the 800 K emitter:

$$(\lambda T)_1 = 0.4 \mu\text{m} \times 800 \text{ K} = 320 \mu\text{m} \cdot \text{K} \text{ and } F_{0 \rightarrow \lambda_1} = 0.000000$$

$$(\lambda T)_2 = 0.7 \mu\text{m} \times 800 \text{ K} = 560 \mu\text{m} \cdot \text{K} \text{ and } F_{0 \rightarrow \lambda_2} = 0.000000$$

$$F_{\lambda_1 \rightarrow \lambda_2} = F_{0 \rightarrow \lambda_2} - F_{0 \rightarrow \lambda_1} = 0.000000 - 0.000000 = 0.000000$$

Since the fraction of radiant between 0.4 and 0.7 μm is 0 (to six decimal places), the heater would not appear to be “glowing” at 800 K.

For the 1429 K emitter:

$$(\lambda T)_1 = 0.4 \mu\text{m} \times 1429 \text{ K} = 572 \mu\text{m} \cdot \text{K} \text{ and } F_{0 \rightarrow \lambda_1} = 0.000000$$

$$(\lambda T)_2 = 0.7 \mu\text{m} \times 1429 \text{ K} = 1000 \mu\text{m} \cdot \text{K} \text{ and } F_{0 \rightarrow \lambda_2} = 0.000321$$

$$F_{\lambda_1 \rightarrow \lambda_2} = F_{0 \rightarrow \lambda_2} - F_{0 \rightarrow \lambda_1} = 0.000321 - 0.000000 = 0.000321$$

Since the emission fraction in the visible range is nonzero (albeit very small) the heater would appear to be glowing (if it didn’t melt first).

Radiant Intensity and Heat Flux

When analyzing fire phenomena, we usually speak in terms of heat fluxes. For example, a radiant heat flux (\dot{q}_r'') of 20 kW/m² to the floor is often quoted as a rule of thumb for determining the onset of flashover in a compartment. Consider a target located on the floor of a compartment as it approaches flashover: the radiant heat flux “felt” by this target is the sum of all thermal radiation incident on this target, regardless of where the radiation originated. Some of the radiation incident to the target may have been emitted by flames, another part may have been emitted by the ceiling or walls, and another part may have been emitted by soot particles located in the hot gas layer. Thus, incident radiation comes in from all directions and the radiation felt by the target passes through an imaginary hemisphere surrounding the target. The radiant intensity passing through different parts of this hemisphere will, in general, vary spatially. The radiant intensity passing through part of the hemisphere facing the flames is likely greater than the radiant intensity passing through part of the hemisphere facing away from the flames. It is seen that in order properly analyze a radiant heat transfer problem, it is necessary to take into account the directional nature of radiation. The concept of *radiant intensity* is introduced as a tool to analyze the directional nature of thermal radiation.

Radiant intensity is defined on a per unit solid angle (Ω , sr or steradians) basis. The surface area

of a sphere having radius r is $4\pi r^2$ and a unit sphere, i.e. a sphere with a radius of 1, has a surface area of 4π . The solid angle subtended by a surface is the area of a unit sphere covered by the surface’s projection onto that unit sphere. For example, a hemisphere subtends a solid angle of 2π steradians, and all space subtends a solid angle of 4π steradians. Referring to the spherical coordinate system in Fig. 4.3, the differential solid angle $d\Omega$ is defined as:

$$d\Omega = \frac{dA}{|R|^2} = \sin(\theta)d\theta d\phi \quad (4.7)$$

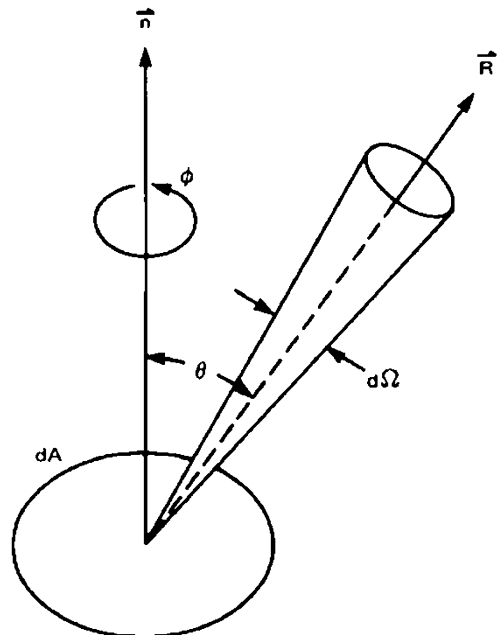


Fig. 4.3 Coordinate system for radiation intensity

where ϕ is azimuthal angle (radians), θ is polar angle (radians), and dA is the differential area normal to the θ and ϕ directions. In simple terms, ϕ can be thought of as degrees longitude and θ can be thought of as degrees latitude on a globe.

Spectral radiant intensity ($\text{W/m}^2 \cdot \text{sr} \cdot \mu\text{m}$) is an inherently directional quantity defined as radiant power per unit area normal to the emitting surface per unit solid angle per unit wavelength:

$$I_\lambda(\lambda, \theta, \phi) = \frac{d\dot{q}}{dA \cdot d\Omega \cdot d\lambda} \quad (4.8)$$

The radiant heat flux at a single wavelength across a surface of an arbitrary orientation is the spectral radiant heat flux [5, 6]:

$$\begin{aligned} \dot{q}_\lambda''(\lambda) &= \int_0^{4\pi} I_\lambda(\lambda, \theta, \phi) \cos(\theta) d\Omega \\ &= \int_0^{2\pi} \int_0^{\pi/2} I_\lambda(\lambda, \theta, \phi) \cos(\theta) \sin(\theta) d\theta d\phi \end{aligned} \quad (4.9)$$

where I_λ is the radiation intensity at wavelength λ per unit solid angle (Fig. 4.3). Intensity is a useful measure for thermal radiation because the intensity of a radiant beam remains constant if it is traveling through a nonparticipating medium. The total radiant heat flux is obtained by integrating Equation 4.9 over all wavelengths:

$$\dot{q}_r'' = \int_0^\infty \dot{q}_\lambda''(\lambda) d\lambda \quad (4.10)$$

The salient point here is that radiant intensity is not the same as radiant heat flux. Radiant

intensity is a directional (and possibly spectral) quantity. Radiant heat flux is obtained by summing (or integrating) individual contributions over all directions (Equation 4.9) and usually wavelengths (Equation 4.10).

Emission, Irradiation, and Radiosity

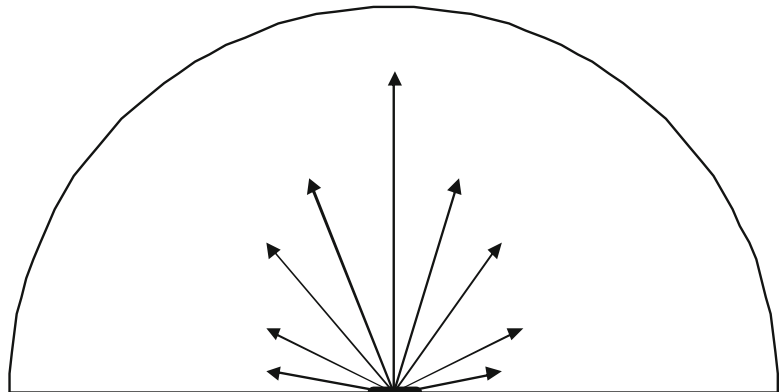
Emission

Now define $I_{\lambda,e}(\lambda, \theta, \phi)$ as the spectral intensity of radiation emitted by a surface (subscript “e” means emission or emitted). The emissive power of that surface at wavelength λ is defined in an analogous manner to Equation 4.9, but with \dot{q}_λ'' replaced by E_λ and I_λ replaced by $I_{\lambda,e}$:

$$\begin{aligned} E_\lambda(\lambda) &= \int_0^{4\pi} I_{\lambda,e}(\lambda, \theta, \phi) \cos(\theta) d\Omega \\ &= \int_0^{2\pi} \int_0^{\pi/2} I_{\lambda,e}(\lambda, \theta, \phi) \cos(\theta) \sin(\theta) d\theta d\phi \end{aligned} \quad (4.11)$$

It is seen that for a surface at a given temperature, the intensity of emitted radiation depends on wavelength and direction. For engineering applications, this directional dependency of surface emission is usually neglected and we instead (implicitly or explicitly) work with *hemispherical* radiation emission. Hemispherical emission can be envisioned by picturing a small (differential) element located at the center of an imaginary hemispherical enclosure (see Fig. 4.4). Due to the directional dependency of surface emission, the intensity of radiation emitted

Fig. 4.4 Directional emission from a differential surface. Length of arrows represents spectral directional intensity of emitted thermal radiation



by this surface that impinges on the imaginary hemispherical enclosure may vary with location. However, for engineering purposes, it is usually adequate to neglect the potentially directional character of surface emission and consider only hemispherical emission, meaning the radiant emission that impinges on some part of the imaginary hemispherical enclosure. In practice, this is equivalent to assuming that a surface is a diffuse emitter, meaning the intensity of emitted radiation is independent of direction.

For the reasons described above, in most engineering applications surfaces are approximated as diffuse, which means that $I_{\lambda,e}$ is a constant that does not vary with θ and ϕ , even though emission of thermal radiation from all real surfaces exhibits some directional dependency. Under this diffuse approximation $I_{\lambda,e}$ can be removed from the integrand in Equation 4.11:

$$\begin{aligned} E_{\lambda}(\lambda) &= \int_0^{2\pi} \int_0^{\pi/2} I_{\lambda,e}(\lambda, \theta, \phi) \cos(\theta) \sin(\theta) d\theta d\phi \\ &= I_{\lambda,e}(\lambda) \int_0^{2\pi} \int_0^{\pi/2} \cos(\theta) \sin(\theta) d\theta d\phi \\ &= \pi I_{\lambda,e}(\lambda) \end{aligned} \quad (4.12)$$

and it is seen that the emissive power of a diffuse surface equals its spectral intensity multiplied by π steradians (for diffuse surfaces $E = \pi I$ and for this reason Equation 4.4 can also be written as $E_{\lambda,b}(\lambda, T) = \pi I_{\lambda,b}(\lambda, T)$). The total emissive power is obtained by integrating over all wavelengths:

$$E = \int_0^{\infty} E_{\lambda}(\lambda) d\lambda = \pi I_e \quad (4.13)$$

An important result that is obtained from Equation 4.4 after performing the integration in Equation 4.13 is the Stefan-Boltzman Law, already presented as Equation 4.5.

For a diffuse surface, the fraction of radiation emitted in angle range $\phi_1 \leq \phi \leq \phi_2$ and $\theta_1 \leq \theta \leq \theta_2$ can be calculated as:

$$F(\theta_1, \theta_2, \phi_1, \phi_2) = \frac{1}{\pi} \int_{\phi_1}^{\phi_2} \int_{\theta_1}^{\theta_2} \cos(\theta) \sin(\theta) d\theta d\phi \quad (4.14)$$

Example 3 What is the emissive power of a blackbody at 1000 K? What is its emissive power between 1 and 5 μm for all emission angles? What is its emissive power between 1 and 5 μm for $0 \leq \phi \leq 2\pi$ and $0 \leq \theta \leq \pi/4$?

Solution Blackbody emissive power is calculated from Equation 4.5:

$$\begin{aligned} E_b &= \sigma T^4 = 5.67 \times 10^{-8} \times 1000^4 \\ &= 56.7 \text{ kW/m}^2 \end{aligned}$$

The fraction of this radiation emitted at wavelengths between 1 and 5 μm can be calculated with Equation 4.6 and Table 4.1 as follows:

$$(\lambda T)_1 = 1 \mu\text{m} \times 1000 \text{ K} = 1000 \mu\text{m} \cdot \text{K} \text{ and } F_{0 \rightarrow \lambda_1} = 0.000321$$

$$(\lambda T)_2 = 5 \mu\text{m} \times 1000 \text{ K} = 5000 \mu\text{m} \cdot \text{K} \text{ and } F_{0 \rightarrow \lambda_2} = 0.633747$$

$$F_{\lambda_1 \rightarrow \lambda_2} = F_{0 \rightarrow \lambda_2} - F_{0 \rightarrow \lambda_1} = 0.633747 - 0.000321 = 0.633426$$

The emissive power between 1 and 5 μm , for all emission angles, is $56.7 \text{ kW/m}^2 \times 0.633 = 35.9 \text{ kW/m}^2$.

The fraction of radiation emitted in the direction $0 \leq \phi \leq 2\pi$ and $0 \leq \theta \leq \pi/4$ can be calculated from Equation 4.14 as:

$$F(\theta_1, \theta_2, \phi_1, \phi_2) = \frac{1}{\pi} \int_0^{2\pi} \int_0^{\pi/4} \cos(\theta) \sin(\theta) d\theta d\phi$$

$$\begin{aligned} F(\theta_1, \theta_2, \phi_1, \phi_2) &= \frac{1}{\pi} \int_0^{2\pi} \left(-\frac{1}{2} \cos^2(\theta) \Big|_{\theta=0}^{\theta=\pi/4} \right) d\phi \\ &= \frac{1}{4\pi} \int_0^{2\pi} d\phi = \frac{2\pi}{4\pi} = 0.5 \end{aligned}$$

The emissive power between 1 and 5 μm for this angle range is $35.9 \text{ kW/m}^2 \times 0.5 = 18 \text{ kW/m}^2$.

Irradiation

Spectral irradiation $G_\lambda(\lambda)$ ($\text{W/m}^2 \cdot \mu\text{m}$) is the radiant heat flux at wavelength λ to a surface incident from all directions. It is obtained by integrating the incident spectral radiation intensity over all angles in a manner directly analogous to the way that spectral emissive power was defined in Equation 4.11:

$$G_\lambda(\lambda) = \int_0^{2\pi} \int_0^{\pi/2} I_{\lambda,i}(\lambda, \theta, \phi) \cos(\theta) \sin(\theta) d\theta d\phi \quad (4.15)$$

Total irradiation (G , W/m^2) is obtained by integrating G_λ over all wavelengths:

$$G = \int_0^\infty G_\lambda(\lambda) d\lambda \quad (4.16)$$

Note that G_λ has no subscript i (for incident) because by definition irradiation is incident on a surface so the “ i ” would be redundant. G is the total radiant heat flux incident to a target.

Example 4 A surface is uniformly irradiated with a source having the following characteristics:

$$G_\lambda = 0 \text{ kW/m}^2 \cdot \mu\text{m} \text{ for } \lambda \leq 2 \mu\text{m}$$

$$G_\lambda = 5 \text{ kW/m}^2 \cdot \mu\text{m} \text{ for } 2 < \lambda \leq 8 \mu\text{m}$$

$$G_\lambda = 10 \text{ kW/m}^2 \cdot \mu\text{m} \text{ for } 8 < \lambda \leq 20 \mu\text{m}$$

$$G_\lambda = 0 \text{ kW/m}^2 \cdot \mu\text{m} \text{ for } \lambda > 20 \mu\text{m}$$

What is its total irradiation?

Solution Total irradiation can be calculated from Equation 4.16 as:

$$\begin{aligned} G &= \int_0^\infty G_\lambda(\lambda) d\lambda = \int_2^8 5 d\lambda + \int_8^{20} 10 d\lambda \\ &= 5 \times (8 - 2) + 10 \times (20 - 8) \\ &= 150 \text{ kW/m}^2 \end{aligned}$$

Radiosity

As will be discussed later, a certain fraction of radiation impinging on a surface may be reflected by that surface. Thus, the total amount of radiation leaving a surface is the sum of the radiation emitted by that surface plus the radiation reflected by that surface. The total radiation leaving a surface, whether emitted or reflected, is called radiosity, J .

Spectral radiosity J_λ is:

$$J_\lambda(\lambda) = \int_0^{2\pi} \int_0^{\pi/2} I_{\lambda,e,r}(\lambda, \theta, \phi) \cos(\theta) \sin(\theta) d\theta d\phi \quad (4.17)$$

Total radiosity (J , W/m^2) is obtained by integrating J_λ over all wavelengths:

$$J = \int_0^\infty J_\lambda(\lambda) d\lambda \quad (4.18)$$

Surface Properties

Thermal radiation may be absorbed at, reflected by, or transmitted through a surface. Imprecisely, absorptivity (α) is the fraction absorbed at the surface, reflectivity (ρ) is the fraction reflected by the surface, and transmissivity (τ) is the fraction transmitted through the surface. It follows from a radiation balance:

$$\alpha + \rho + \tau = 1 \quad (4.19)$$

where each property in Equation 4.29 may exhibit spectral and directional characteristics

(but such dependency is not explicitly shown). Additionally, emissivity (ϵ) is the ratio of the actual amount of radiation emitted by a surface to the maximum possible amount of radiation that could be emitted by that surface if it was a blackbody. These properties are defined more precisely in the sections that follow.

Emissivity

Since no surface can emit more thermal radiation than a blackbody, a logical tool for normalizing thermal emission from real surfaces is the blackbody. Spectral surface emissivity is defined as the ratio of the actual spectral intensity of radiation emitted by a surface to the blackbody spectral intensity:

$$\epsilon_{\lambda}(\lambda, \theta, \phi, T) = \frac{I_{\lambda, e}(\lambda, \theta, \phi, T)}{I_{\lambda, b}(T)} \quad (4.20)$$

As described earlier, hemispherical radiation quantities are usually applied in engineering applications. The spectral hemispherical emissivity is defined in terms of the blackbody emissive power at wavelength λ and is obtained by integrating Equation 4.20 over all directions with the result:

$$\epsilon_{\lambda}(\lambda, T) = \frac{E_{\lambda}(\lambda, T)}{E_{\lambda, b}(\lambda, T)} \quad (4.21)$$

Spectral normal emissivity (very close to hemispherical emissivity) is shown for several materials in Fig. 4.5 [4].

Total emissivity is obtained by integrating Equation 4.21 over all wavelengths:

$$\epsilon(T) = \frac{E(T)}{E_b(T)} \quad (4.22)$$

By definition, the emissivity of a blackbody (whether $\epsilon_{\lambda}(\lambda, \theta, \phi, T)$, $\epsilon_{\lambda}(\lambda, T)$, or $\epsilon(T)$) is unity. Total normal emissivity (very close to hemispherical emissivity) is shown graphically in Fig. 4.6 for several materials [4]. Representative values of total hemispherical emissivity are tabulated for several materials in Table 4.2 [7] (metals) and Table 4.3 [7] (non-metals).

Absorptivity

In a fire, one of the most important radiative characteristics of a material or surface is its absorptivity, defined loosely as the fraction of the incident radiation that is absorbed by the material. The absorptivity is strongly

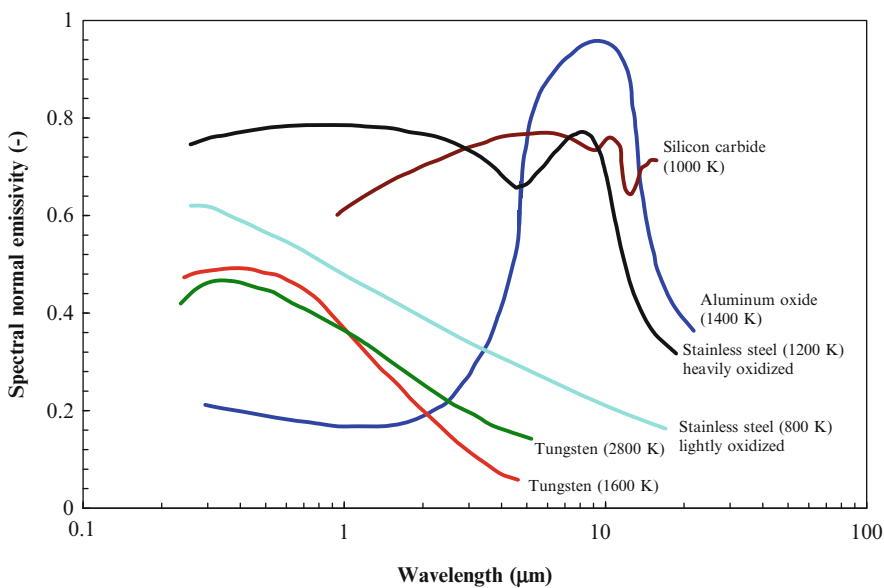


Fig. 4.5 Spectral normal emissivity of several materials [4]

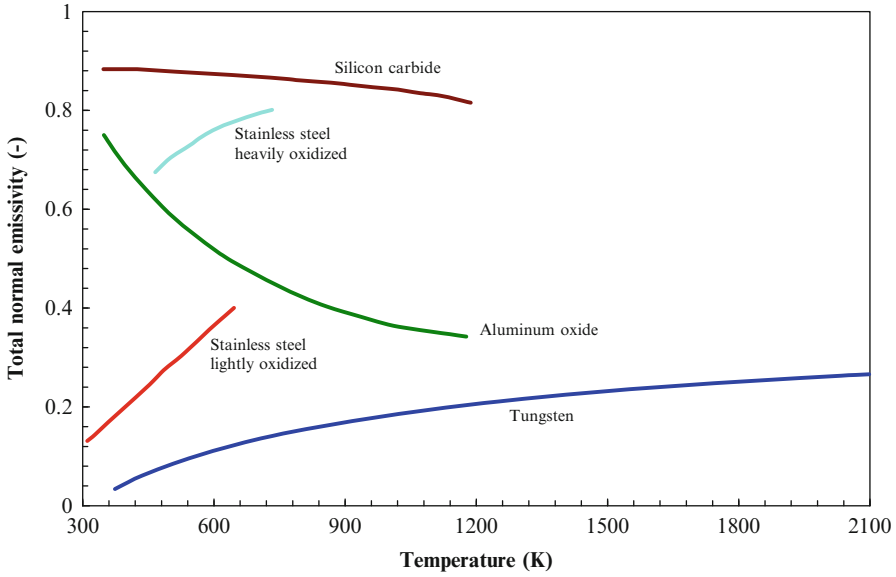


Fig. 4.6 Total normal emissivity of several materials [4].

Table 4.2 Representative total hemispherical emissivity of several metals [7]

Material	Description	Emissivity
Aluminum	Crude	0.07–0.08 (0–200 °C)
	Foil, bright	0.01 (–9 °C), 0.04 (1 °C), 0.087 (200 °C)
	Highly polished	0.04–0.05 (1 °C)
	Ordinarily rolled	0.035 (100 °C), 0.05 (500 °C)
	Oxidized	0.11 (200 °C), 0.19 (600 °C)
	Roughed	0.044–0.066 (40 °C)
	Unoxidized	0.022 (25 °C), 0.06 (500 °C)
Bismuth	Unoxidized	0.048 (25 °C), 0.061 (100 °C)
Brass	After rolling	0.06 (30 °C)
	Browned	0.5 (20–300 °C)
	Polished	0.03 (300 °C)
Chromium	Polished	0.07 (150 °C)
	Unoxidized	0.08 (100 °C)
Cobalt	Unoxidized	0.13 (500 °C), 0.23 (1000 °C)
Copper	Black oxidized	0.78 (40 °C)
	Highly polished	0.03 (1 °C)
	Molten	0.15
	Matte	0.22 (40 °C)
	New	0.07 (40–100 °C)
	Oxidized	0.56 (40–200 °C), 0.61 (200 °C), 0.88 (540 °C)
	Polished	0.04 (40 °C), 0.05 (260 °C), 0.17 (1100 °C)
Rolled	0.64 (40 °C)	
Gold	Polished	0.02 (40 °C), 0.03 (1100 °C)
	Electrolytically deposited	0.02 (40 °C), 0.03 (1100 °C)

(continued)

Table 4.2 (continued)

Material	Description	Emissivity
Inconel	Sandblasted	0.79 (800 °C), 0.91 (1150 °C)
	Stably oxidized	0.69 (300 °C), 0.82 (1000 °C)
	Untreated	0.3 (40–260 °C)
	Rolled	0.69 (300 °C), 0.88 (1150 °C)
Inconel X	Stably oxidized	0.89 (300 °C), 0.93 (1100 °C)
Iron	Cast	0.21 (40 °C)
	Cast, freshly turned	0.44 (40 °C), 0.7 (1100 °C)
	Galvanized	0.22–0.28 (0–200 °C)
	Molten	0.02–0.05 (1100 °C)
	Plate, rusted red	0.61 (40 °C)
	Pure polished	0.06 (40 °C), 0.13 (540 °C)
	Red iron oxide	0.96 (40 °C), 0.67 (540 °C)
	Rough ingot	0.95 (1100 °C)
	Smooth sheet	0.6 (1100 °C)
	Wrought, polished	0.28 (40–260 °C)
Lead	Oxidized	0.28 (00–200 °C)
	Unoxidized	0.05 (100 °C)
Magnesium		0.13 (260 °C), 0.18 (310 °C)
Mercury		0.09 (0 °C), 0.12 (100 °C)
Molybdenum	Oxidized	0.78–0.81 (300–540 °C)
Monel	Oxidized	0.43 (20 °C)
	Polished	0.09 (20 °C)
Nichrome	Rolled	0.36 (800 °C), 0.8 (1150 °C)
	Sandblasted	0.81 (800 °C), 0.87 (1150 °C)
Nickel	Electrolytic	0.04 (40 °C), 0.1 (540 °C)
	Oxidized	0.31–0.39 (40 °C), 0.67 (540 °C)
	Wire	0.1 (260 °C), 0.19 (1100 °C)
Platinum	Oxidized	0.07 (260 °C), 0.11 (540 °C)
	Unoxidized	0.04 (25 °C), 0.05 (100 °C), 0.15 (1000 °C)
Silver	Polished	0.01 (40 °C), 0.02 (260 °C), 0.03 (540 °C)
Steel	Calorized	0.5–0.56 (40–540 °C)
	Cold rolled	0.08 (100 °C)
	Ground sheet	0.61 (1100 °C)
	Oxidized	0.79 (260–540 °C)
	Plate, rough	0.94–0.97 (40–540 °C)
	Polished	0.07 (40 °C), 0.1 (260 °C), 0.14 (540 °C), 0.23 (1100 °C)
	Rolled sheet	0.66 (40 °C)
	Type 347, oxidized	0.87–0.91 (300–1100 °C)
	Type AISI 303, oxidized	0.74–0.87 (300–1100 °C)
	Type 310, oxidized & rolled	0.56 (800 °C), 0.81 (1150 °C)
Sandblasted	0.82 (800 °C), 0.93 (1150 °C)	
Stellite		0.18 (20 °C)
Tantalum		0.19 (1300 °C)
Tin	Unoxidized	0.04–0.05 (25–100 °C)
Tungsten	Filament	0.18 (40 °C), 0.11 (540 °C), 0.39 (2800 °C)
Zinc	Oxidized	0.11 (260 °C)
	Polished	0.02 (40 °C), 0.03 (260 °C)

Table 4.3 Representative total hemispherical emissivity of several non-metals [7]

Material	Description	Emissivity	
Bricks	Chrome refractory	0.94 (540 °C), 0.98 (1100 °C)	
	Fire clay	0.75 (1400 °C)	
	Light buff	0.8 (540 °C)	
	Magnesite refractory	0.38 (1000 °C)	
	Sand lime red	0.59 (1400 °C)	
	Silica	0.84 (1400 °C)	
	Various refractories	0.71–0.88 (1100 °C)	
	White refractory	0.89 (260 °C), 0.68 (540 °C)	
Building materials	Asbestos, board	0.96 (40 °C)	
	Asphalt pavement	0.85–0.93 (40 °C)	
	Clay	0.39 (20 °C)	
	Concrete, rough	0.94 (0–100 °C)	
	Granite	0.44 (40 °C)	
	Gravel	0.28 (40 °C)	
	Gypsum	0.9 (40 °C)	
	Marble, polished	0.93 (40 °C)	
	Mica	0.75 (40 °C)	
	Plaster	0.89 (40 °C), 0.48 (540 °C)	
	Quartz	0.76 (40 °C)	
	Sand	0.83 (40 °C)	
	Sandstone	0.83 (40 °C)	
	Slate	0.67 (40–260 °C)	
Carbon	Baked	0.52–0.79 (1000–2400 °C)	
	Filament	0.95 (260 °C)	
	Graphitized	0.76–0.71 (100–500 °C)	
	Rough	0.77 (100–320 °C)	
	Soot (candle)	0.95 (120 °C)	
	Soot (coal)	0.95 (20 °C)	
	Unoxidized	0.8 (25–500 °C)	
Ceramics	Alumina coating on inconel	0.65 (430 °C), 0.45 (1100 °C)	
	Zirconia coating on inconel	0.62 (430 °C), 0.45 (1100 °C)	
	Earthenware, glazed	0.9 (1 °C)	
	Earthenware, matte	0.93 (1 °C)	
	Procelain	0.92 (40 °C)	
	Refractory, black	0.94 (100 °C)	
	Refractory, light buff	0.92 (100 °C)	
	Refractory, white	0.9 (100 °C)	
	Al ₂ O ₃		
Cloth	Cotton	0.77 (20 °C)	
	Silk	0.78 (20 °C)	
Glass	Convex D	0.8–0.76 (100–500 °C)	
	Fused quartz	0.75–0.8 (100–500 °C)	
	Nonex	0.82–0.78 (100–500 °C)	
	Pyrex	0.8–0.9 (40 °C)	
	Smooth	0.92–0.95 (0–200 °C)	
	Waterglass	0.96 (20 °C)	
	Ice	Smooth	0.92 (0 °C)
	Oxides	Al ₂ O ₃	0.35–0.54 (850–1300 °C)
		C ₂ O	0.27 (850–1300 °C)
		Cr ₂ O ₃	0.73–0.95 (850–1300 °C)
		Fe ₂ O ₃	0.57–0.78 (850–1300 °C)
		MgO	0.29–0.5 (850–1300 °C)
		NiO	0.52–0.86 (500–1200 °C)
		ZnO	0.3–0.65 (850–1300 °C)
Paints	Aluminum	0.27–0.7 (1–100 °C)	
	Enamel, snow white	0.91 (40 °C)	
	Lacquer	0.85–0.93 (40 °C)	
	Lampblack	0.94–0.97 (40 °C)	
	Oil	0.89–0.97 (0–200 °C)	
Paper	White	0.89–0.97 (40 °C)	
	White	0.95 (40 °C), 0.82 (540 °C)	
Roofing materials	Aluminum surfaces	0.22 (40 °C)	
	Asbestos cement	0.65 (1400 °C)	
	Bituminous felt	0.89 (1400 °C)	
	Enameled steel, white	0.65 (1400 °C)	
	Galvanized iron, dirty	0.90 (1400 °C)	
	Galvanized iron, new	0.42 (1400 °C)	
	Roofing sheet, brown	0.8 (1400 °C)	
	Roofing sheet, green	0.87 (1400 °C)	
	Tiles, uncolored	0.63 (1400 °C)	
	Tiles, brown	0.87 (1400 °C)	
	Tiles, black	0.94 (1400 °C)	
Tiles, asbestos cement	0.66 (1400 °C)		
Weathered asphalt	0.88 (1400 °C)		

(continued)

Table 4.3 (continued)

Material	Description	Emissivity
Rubber	Hard, black, glossy	0.95 (40 °C)
	Soft, gray	0.86 (40 °C)
Snow	Fine	0.82 (−10 °C)
	Frost	0.98 (0 °C)
	Granular	0.89 (−10 °C)
Soils	Black loam	0.66 (20 °C)
	Plowed field	0.38 (20 °C)
Water		0.92–0.96 (0–40 °C)
Wood	Beech	0.91 (70 °C)
	Oak, planed	0.91 (40 °C)
	Sawdust	0.75 (40 °C)
	Spruce, sanded	0.82 (100 °C)

wavelength-dependent. For example, at wavelengths below 1 μm the absorptivity of clear Polymethylmethacrylate is close to zero, but at wavelengths above 3 μm it approaches unity.

A blackbody absorbs all incident radiation with no spectral or directional dependency. As with emissivity, the idealized blackbody behavior is used as a normalization tool to quantify the amount of radiation absorbed by a surface relative to the maximum possible amount the surface may absorb (i.e., if it was a blackbody).

Spectral radiant intensity incident on a surface is denoted $I_{\lambda,i}$; it is, in general, a function of λ , θ , and ϕ . Spectral, directional absorptivity is the ratio of the spectral directional radiant intensity absorbed by a surface $I_{\lambda,i,abs}(\lambda, \theta, \phi)$ to the spectral directional radiant intensity incident on that surface $I_{\lambda,i}(\lambda, \theta, \phi)$ (because the latter is the maximum possible radiation that could be absorbed by that surface, i.e. if it was a blackbody):

$$\alpha_{\lambda}(\lambda, \theta, \phi) = \frac{I_{\lambda,i,abs}(\lambda, \theta, \phi)}{I_{\lambda,i}(\lambda, \theta, \phi)} \quad (4.23)$$

Spectral hemispherical absorptivity, a directionally-averaged property that is obtained by integrating over all incident angles, is the ratio of the spectral irradiation absorbed by the surface ($G_{\lambda,abs}$) to the spectral irradiation of the surface G_{λ} :

$$\begin{aligned} \alpha_{\lambda}(\lambda) &= \frac{\int_0^{2\pi} \int_0^{\pi/2} I_{\lambda,i,abs}(\lambda, \theta, \phi) \cos(\theta) \sin(\theta) d\theta d\phi}{\int_0^{2\pi} \int_0^{\pi/2} I_{\lambda,i}(\lambda, \theta, \phi) \cos(\theta) \sin(\theta) d\theta d\phi} \\ &= \frac{G_{\lambda,abs}(\lambda)}{G_{\lambda}(\lambda)} \end{aligned} \quad (4.24)$$

Finally, total hemispherical absorptivity is obtained by integrating spectral hemispherical absorptivity over all wavelengths:

$$\begin{aligned} \alpha &= \frac{\int_0^{\infty} G_{\lambda,abs}(\lambda) d\lambda}{\int_0^{\infty} G_{\lambda}(\lambda) d\lambda} = \frac{\int_0^{\infty} \alpha_{\lambda}(\lambda) G_{\lambda}(\lambda) d\lambda}{\int_0^{\infty} G_{\lambda}(\lambda) d\lambda} \\ &= \frac{G_{abs}}{G} \end{aligned} \quad (4.25)$$

Example 5 A particular diffuse material is idealized as having a spectral absorptivity of zero for wavelengths less than 3 μm and unity for wavelengths greater than 3 μm . Calculate its total hemispherical absorptivity for a blackbody at 800, 1200, and 2000 K.

Solution Assume $G_{\lambda}(\lambda) = E_{\lambda,b}(\lambda, T_e)$ where T_e is the temperature of the emitter (800, 1200, and 2000 K) and use Equation 4.25:

$$\alpha(T_e) = \frac{\int_0^{\infty} \alpha_{\lambda}(\lambda) E_{\lambda,b}(\lambda, T_e) d\lambda}{\int_0^{\infty} E_{\lambda,b}(\lambda, T_e) d\lambda} = \frac{\int_0^3 0 \times E_{\lambda,b}(\lambda, T_e) d\lambda + \int_3^{\infty} 1 \times E_{\lambda,b}(\lambda, T_e) d\lambda}{\sigma T_e^4} = \frac{\int_3^{\infty} E_{\lambda,b}(\lambda, T_e) d\lambda}{\sigma T_e^4}$$

It is possible to put this in a form that allows use of the radiation fraction tabulated in Table 4.1:

$$\begin{aligned}\alpha &= \frac{\int_0^\infty E_{\lambda,b}(\lambda, T_e) d\lambda - \int_0^3 E_{\lambda,b}(\lambda, T_e) d\lambda}{\sigma T_e^4} \\ &= \frac{\sigma T_e^4 - \int_0^3 E_{\lambda,b}(\lambda, T_e) d\lambda}{\sigma T_e^4} \\ &= 1 - \frac{\int_0^3 E_{\lambda,b}(\lambda, T_e) d\lambda}{\sigma T_e^4} = 1 - F_{0 \rightarrow 3}(3T_e)\end{aligned}$$

For $T_e = 800$ K, $\lambda T_e = 2400 \mu\text{m} \cdot \text{K}$ and from

Table 4.1 $F_{0 \rightarrow 3} = 0.14$ so $\alpha = 0.86$.

For $T_e = 1200$ K, $\lambda T_e = 3600 \mu\text{m} \cdot \text{K}$ and from

Table 4.1 $F_{0 \rightarrow 3} = 0.40$ so $\alpha = 0.60$.

For $T_e = 2000$ K, $\lambda T_e = 6000 \mu\text{m} \cdot \text{K}$ and from

Table 4.1 $F_{0 \rightarrow 3} = 0.76$ so $\alpha = 0.24$.

It is seen that, for this idealized material, the effective absorptivity is a strong function of emitter temperature.

In a fire we are usually interested in the total hemispherical absorptivity defined in Equation 4.25. However, as demonstrated above, the total hemispherical absorptivity depends on the spectral energy distribution of the radiation source. Therefore, a material technically cannot be assigned a single absorptivity value because the spectral distribution of the incoming radiation depends on the temperature of the emitter. Due to Wien's displacement law and the Planck distribution, this is true even if the emitter behaves as a blackbody. In fires, the temperature of radiation sources ranges from approximately ~ 600 K (smoke layer, hot surfaces) to ~ 2000 K (flames). Additionally, certain bench-scale fire tests use tungsten-filament heaters that operate at temperatures near 3000 K. Thus, the effect of source temperature on the integrated (or effective) absorptivity has relevance for both real fires and bench-scale fire testing.

Hallman's 1971 Ph.D. dissertation [8] and subsequent publications [9, 10] remain some of the most comprehensive sources of information on the change of polymers' total hemispherical absorptivity with the temperature of the emitter. Hallman measured the spectral absorptivity of

several solids and then determined the integrated surface absorptivity of different solids irradiated by hexane flames, blackbodies between 1000 and 3500 K, and solar energy. His absorptivity data are reproduced in Table 4.4. Note that the total hemispherical absorptivity of some materials is relatively insensitive to the temperature of the radiation source (black PMMA) but others are quite sensitive. For example, the absorptivity of clear PMMA decreases from 0.85 for a 1000 K blackbody to 0.25 for a 3500 K blackbody.

Similar measurements were made by Wesson et al. [11] for undegraded wood. Their results are reproduced in Table 4.5. More recently, Försth and Roos [12] conducted similar measurements for wood products (Table 4.6), carpet (Table 4.7), painted plywood (Table 4.8), and plastics (Table 4.9).

During a fire, a material's radiative characteristics may change. Although the integrated absorptivities from Wesson et al. [11] (reproduced in Table 4.5) are relatively low, the absorptivity of charred wood is generally not the same as that of virgin wood. Janssens [13] suggested that blackening causes the absorptivity of wood to increase from ~ 0.76 (based on Reference [11]) to approximately unity as the surface temperature approaches the ignition temperature. He therefore used an average value of 0.88 in his ignition analyses, and recommends using an integrated absorptivity of 1.0 during flaming combustion [14]. Interestingly, Försth and Roos [12] noted the opposite trend, i.e. a reduction in effective absorptivity as wood darkens. More research is needed in this area.

Wood is not the only class of materials that exhibits a change in radiative characteristics during a fire. Under nonflaming conditions, low density polyethylene has been observed to change from visually opaque to transparent, eventually followed by a darkening of the surface [15]. This indicates that a change in the material's radiative characteristics occurred (at least in the visible range). Modak and Croce [16] reported that for clear PMMA, 39 % of flame radiation is transmitted through the surface, but for "charred" PMMA (previously exposed to a fire environment and then cooled) no radiation penetrates in depth. Bubbling

Table 4.4 Integrated surface absorptivities for polymers from Hallman [9]

Generic name	Trade name	Blackbody emitter temperature (K)						Flame
		1000	1500	2000	2500	3000	3500	
Acrylonitrile butadiene styrene	Cyclocac®	0.91	0.86	0.77	0.71	0.65	0.61	0.92
Cellulose acetate butyrate	Uvex®	0.84	0.71	0.56	0.43	0.34	0.27	0.88
Cork		0.64	0.56	0.49	0.46	0.44	0.44	0.60
Melamine/formaldehyde	Formica®	0.91	0.88	0.85	0.82	0.80	0.79	0.91
Nylon 6/6		0.93	0.90	0.86	0.82	0.75	0.71	0.93
Phenolic	Bakelite	0.90	0.86	0.81	0.77	0.75	0.75	0.91
Polycarbonate (rough surface)	Lexan®	0.87	0.83	0.78	0.75	0.72	0.71	0.88
Polyethylene (low density)		0.92	0.88	0.82	0.77	0.72	0.68	0.93
Polymethylmethacrylate (black)	Plexiglas®	0.94	0.94	0.95	0.95	0.95	0.95	0.94
Polymethylmethacrylate (clear)	Plexiglas®	0.85	0.69	0.54	0.41	0.31	0.25	0.89
Polymethylmethacrylate (white)	Plexiglas®	0.91	0.86	0.78	0.70	0.62	0.56	0.92
Polyoxymethylene	Delrin®	0.92	0.86	0.78	0.71	0.64	0.59	0.93
Polyphenylene oxide		0.86	0.78	0.70	0.63	0.57	0.53	0.88
Polypropylene		0.87	0.83	0.78	0.74	0.70	0.68	0.86
Polystyrene (clear)	Styrolux®	0.75	0.60	0.46	0.35	0.28	0.22	0.78
Polystyrene (white)		0.86	0.75	0.63	0.53	0.45	0.40	0.88
Polyurethane thermoplastic	Texin®	0.92	0.89	0.83	0.77	0.72	0.68	0.93
Polyvinyl chloride (clear)		0.81	0.65	0.49	0.38	0.30	0.24	0.85
Polyvinyl chloride (gray)		0.90	0.90	0.89	0.89	0.89	0.89	0.91
PVC/acrylic (gray, rolled)	Kydex®	0.88	0.87	0.86	0.85	0.84	0.83	0.88
PVC/acrylic (red cast)	Kydex®	0.91	0.90	0.89	0.88	0.87	0.86	0.92
Rubber (Buna-N)		0.92	0.93	0.93	0.93	0.93	0.93	0.92
Rubber (Butyl IIR)		0.92	0.93	0.94	0.94	0.95	0.95	0.92
Rubber (natural, gum)		0.88	0.82	0.76	0.72	0.69	0.68	0.89
Rubber (neoprene)		0.91	0.92	0.93	0.93	0.93	0.93	0.91
Rubber (silicone)		0.79	0.66	0.58	0.54	0.52	0.53	0.79

Table 4.5 Integrated surface absorptivity for wood from different emitters (From Wesson et al. [11])

Wood	Flame radiation	Tungsten lamp radiation	Solar radiation
Alaskan cedar	0.76	0.44	0.36
Ash	0.76	0.46	0.36
Balsa	0.75	0.41	0.35
Birch	0.77	0.47	0.39
Cottonwood	0.76	0.48	0.40
Mahogany	0.76	0.49	0.52
Mansonia	0.76	0.47	0.51
Maple	0.76	0.49	0.44
Oak	0.77	0.56	0.49
Redgum	0.77	0.52	0.56
Redwood	0.77	0.51	0.55
Spruce	0.76	0.45	0.35
White pine	0.76	0.49	0.43
Masonite	0.75	0.52	0.61

occurring near the surface of polymers can change their radiative characteristics, but this effect is has not yet been reliably quantified. In a real fire, materials may become coated in soot from flames or a smoke layer, causing their absorptivities to approach unity.

Reflectivity

A fraction of radiation incident on a surface may be reflected. One complicating factor is that reflection may be diffuse, specular, or (most likely) some combination of these two idealizations. A diffuse reflector is a surface for which, analogous to a diffuse emitter, the intensity of reflected radiation is equal in all directions and does not depend on the angle of incoming

Table 4.6 Effective absorptivities for different grey body temperatures for various wood products (From Försth and Roos [12])

Grey body emitter T (K)	674	852	1025	1153	1300	5777
Cone calorimeter irradiation (kWm^{-2})	10	25	50	75	100	Sun
Product	α_{eff}					
Plywood	0.86	0.84	0.81	0.79	0.76	0.40
Dark heat-treated lacquered ash tree floor	0.89	0.88	0.85	0.83	0.80	0.63
Dark heat-treated non-lacquered ash tree floor	0.83	0.81	0.79	0.77	0.74	0.62
Light lacquered ash tree flooring	0.90	0.88	0.86	0.84	0.82	0.40
Light non-lacquered oak flooring	0.86	0.84	0.81	0.80	0.77	0.37
Medium dark lacquered oak flooring	0.91	0.89	0.87	0.85	0.83	0.56
Medium dark non-lacquered oak flooring	0.86	0.84	0.82	0.80	0.77	0.50

Table 4.7 Effective absorptivities for different grey body temperatures for various carpets (From Försth and Roos [12])

Grey body emitter T (K)	674	852	1025	1153	1300	5777
Cone calorimeter irradiation (kWm^{-2})	10	25	50	75	100	Sun
Product	α_{eff}					
Beige PVC carpet	0.92	0.91	0.90	0.89	0.87	0.60
Pink PVC carpet	0.90	0.88	0.86	0.84	0.81	0.39
Red PVC carpet	0.92	0.92	0.91	0.90	0.89	0.80
Blue PVC carpet	0.89	0.87	0.85	0.83	0.80	0.43
Grey PVC carpet	0.90	0.88	0.86	0.84	0.82	0.43
Black PVC carpet	0.93	0.93	0.93	0.93	0.93	0.92
Grey rubber mat	0.91	0.91	0.91	0.91	0.91	0.82
Black rubber mat	0.90	0.90	0.91	0.91	0.91	0.95
White vinyl carpet	0.88	0.86	0.83	0.81	0.79	0.44
Beige vinyl carpet	0.91	0.90	0.89	0.87	0.85	0.51
Brown vinyl carpet	0.90	0.89	0.88	0.88	0.87	0.77
Grey vinyl carpet	0.92	0.91	0.89	0.88	0.87	0.57
Black vinyl carpet	0.93	0.93	0.93	0.93	0.93	0.94
Beige linoleum carpet	0.92	0.91	0.89	0.88	0.86	0.55

radiation. This contrasts to a specular emitter which is an idealized surface where the angle of reflected radiation is equal to the angle of incident radiation, like a billiard ball bouncing off the rail. Rough surfaces approximate diffuse emitters, and polished surfaces are close to specular surfaces. It is seen that, in its most general form, surface reflection is a bidirectional process meaning the intensity of reflected radiation depends not only on the angle of incident radiation, but also on the angle of reflected radiation. As a simplification, we look only at hemispherically-integrated reflection. Then the

spectral directional reflectivity is defined as the ratio of the reflected spectral radiant intensity to the incident spectral radiant intensity:

$$\rho_{\lambda}(\lambda, \theta, \phi) = \frac{I_{\lambda, i, ref}(\lambda, \theta, \phi)}{I_{\lambda, i}(\lambda, \theta, \phi)} \quad (4.26)$$

note that in Equation 4.26, θ and ϕ refer to the direction of the incident radiation, not the reflected radiation (since, for simplification, no consideration is given to the direction of reflected radiation). Spectral hemispherical reflectivity is obtained by integrating over all incident angles:

$$\begin{aligned}\rho_{\lambda}(\lambda) &= \frac{\int_0^{2\pi} \int_0^{\pi/2} I_{\lambda,i,ref}(\lambda, \theta, \phi) \cos(\theta) \sin(\theta) d\theta d\phi}{\int_0^{2\pi} \int_0^{\pi/2} I_{\lambda,i}(\lambda, \theta, \phi) \cos(\theta) \sin(\theta) d\theta d\phi} \\ &= \frac{G_{\lambda,ref}(\lambda)}{G_{\lambda}(\lambda)}\end{aligned}\quad (4.27)$$

Final, total hemispherical reflectivity is obtained by integrating over all wavelengths:

$$\rho = \frac{\int_0^{\infty} G_{\lambda,ref}(\lambda) d\lambda}{\int_0^{\infty} G_{\lambda}(\lambda) d\lambda} = \frac{G_{ref}}{G} \quad (4.28)$$

Transmissivity

Directional spectral transmissivity is defined in an analogous manner to the other radiation properties discussed here:

$$\tau_{\lambda}(\lambda, \theta, \phi) = \frac{I_{\lambda,i,trans}(\lambda, \theta, \phi)}{I_{\lambda,i}(\lambda, \theta, \phi)} \quad (4.29)$$

Hemispherical spectral transmissivity is:

$$\begin{aligned}\tau_{\lambda}(\lambda) &= \frac{\int_0^{2\pi} \int_0^{\pi/2} I_{\lambda,i,trans}(\lambda, \theta, \phi) \cos(\theta) \sin(\theta) d\theta d\phi}{\int_0^{2\pi} \int_0^{\pi/2} I_{\lambda,i}(\lambda, \theta, \phi) \cos(\theta) \sin(\theta) d\theta d\phi} \\ &= \frac{G_{\lambda,trans}(\lambda)}{G_{\lambda}(\lambda)}\end{aligned}\quad (4.30)$$

And total transmissivity is then obtained by integrating over all wavelengths:

$$\tau = \frac{\int_0^{\infty} G_{\lambda,trans}(\lambda) d\lambda}{\int_0^{\infty} G_{\lambda}(\lambda) d\lambda} = \frac{G_{trans}}{G} \quad (4.31)$$

Kirchhoff's Law: Relation Between Emissivity and Absorptivity

Kirchhoff's law is used extensively in radiation heat transfer calculations. In its most general form, Kirchhoff's law states that in order to maintain thermal equilibrium, the spectral directional absorptivity must be equal to the spectral directional emissivity:

$$\alpha_{\lambda}(\lambda, \theta, \phi) = \varepsilon_{\lambda}(\lambda, \theta, \phi, T) \quad (4.32)$$

Using the relations presented earlier in the chapter, it can be shown that if the irradiation is diffuse *or* the surface is diffuse, then Kirchhoff's law has no directional dependency, i.e.:

$$\alpha_{\lambda}(\lambda) = \varepsilon_{\lambda}(\lambda, T) \quad (4.33)$$

If Equation 4.33 applies (i.e., the irradiation is diffuse *or* the surface is diffuse), then if the surface is also *gray* (meaning α_{λ} and ε_{λ} are invariant with λ) *or* the surface is irradiated only by radiation emitted from a blackbody at the same temperature as the surface, its total absorptivity is equal to its total emissivity:

$$\alpha = \varepsilon \quad (4.34)$$

For engineering calculations, Equation 4.34 is most commonly applied for the special case of diffuse and gray surfaces. Fortunately, this is a reasonable approximation for many radiation heat transfer engineering models for participating media in fire applications.

Although real surfaces may exhibit an emissivity that varies with wavelength (see Fig. 4.7), an effective emissivity can be selected so that the integrated emissive power of the gray surface matches the integrated emissive power of the real surface at a particular temperature.

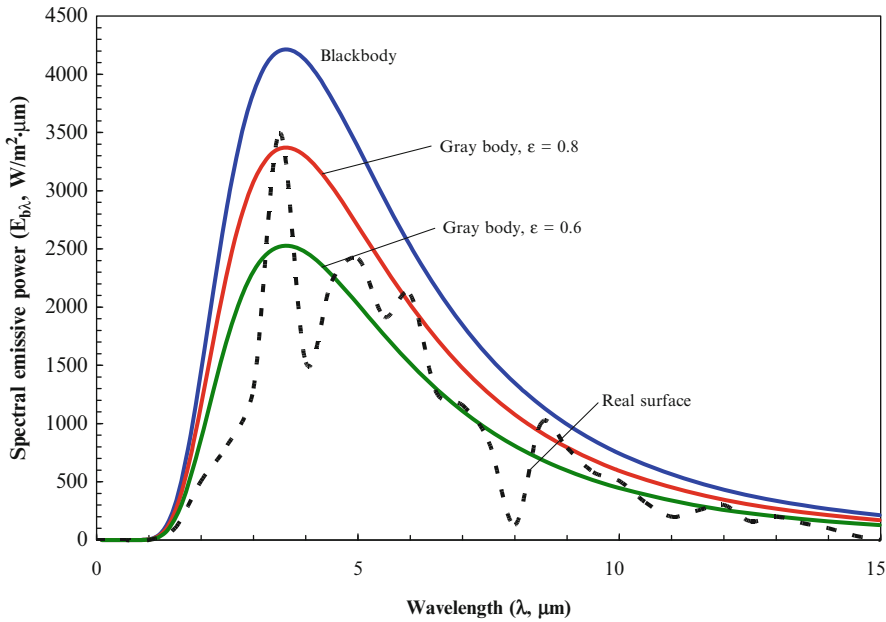


Fig. 4.7 Monochromatic emissive power for black body, two gray bodies, and real surface

Radiant Heat Transfer in Nonparticipating Media

In this section, cases are examined where the surfaces are separated by a medium that does not emit, absorb, or scatter radiation. A vacuum meets this requirement exactly, and common diatomic gases of symmetric molecular structure such as N_2 , O_2 , and H_2 are very nearly nonparticipating media within the thermal radiation spectrum. The radiative energy transfer between the surfaces depends on the geometry, orientation, temperature, and radiation properties of the surfaces. In practice, surfaces are usually idealized as isothermal, diffuse, and gray to make engineering calculations tractable. The geometry and orientation of each surface is commonly accounted for in calculations by one or more configuration factors, also known as view factors, shape factors, angle factors, and geometric factors [1–7, 17–19].

View Factors

A view factor, or configuration factor, is a purely geometrical relation between two surfaces. It is

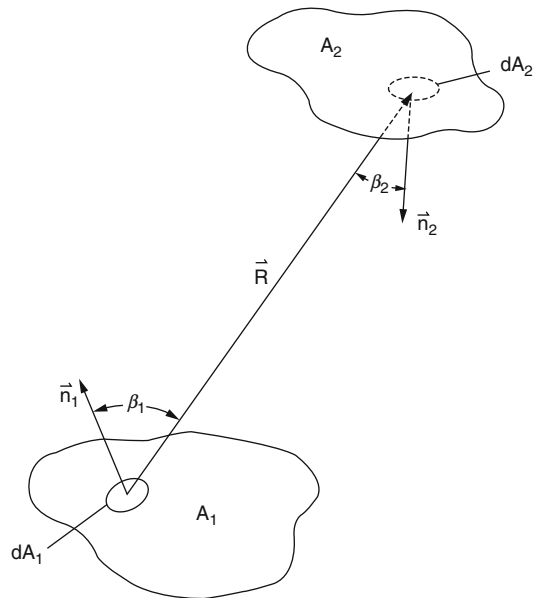


Fig. 4.8 Coordinate system for shape factors

defined as the fraction of radiation leaving one surface which is intercepted by the other surface.

Consider the two arbitrarily oriented surfaces A_1 and A_2 in Fig. 4.8. Assuming that the radiosity from differential area dA_1 is diffuse, the

configuration factor from dA_1 to the finite area A_2 , F_{d1-2} , is given by

$$F_{d1-2} = \int_{A_2} \frac{\cos(\beta_1) \cos(\beta_2)}{\pi |\vec{R}|^2} dA_2 \quad (4.35)$$

where the separation distance between the two surfaces is $|\vec{R}|$, β is the angle between the line of sight \vec{R} and the surface normal \vec{n} , and A_2 is the area of surface 2. If the radiosity from all of surface A_1 (not just differential area dA_1) is diffuse, then the configuration factor for the finite area A_1 to A_2 , F_{1-2} , is calculated as:

$$F_{1-2} = \frac{1}{A_1} \int_{A_1} \int_{A_2} \frac{\cos(\beta_1) \cos(\beta_2)}{\pi |\vec{R}|^2} dA_1 dA_2 \quad (4.36)$$

All configuration factors can be derived using the multiple integration of Equations 4.35 and 4.36, but this is generally very tedious except for simple geometries. Several cases have been tabulated with the numerical results or algebraic formulas available in various references [1–7, 17, 18]. Several configuration factors are provided in Appendix D.

The configuration factors in Appendix D can be extended to other geometries by using configuration factor algebra and the method of surface decomposition. In surface decomposition, unknown factors can be determined from known factors for convenient areas or for imaginary surfaces which can extend real surfaces or form an enclosure [1, 6].

When the radiant fluxes from both surfaces are uniformly and diffusely distributed (a common engineering assumption), a reciprocity relation for any given pair of configuration factors in a group of exchanging surfaces is:

$$A_i F_{i-j} = A_j F_{j-i} \quad (4.37)$$

The summation rule is another useful relation for calculating unknown configuration factors

$$\sum_j F_{i-j} = 1 \quad (4.38)$$

where F_{i-j} relate to surfaces that subtend a closed system. It is possible for a concave surface to “see” itself, which can make F_{i-i} important in certain situations.

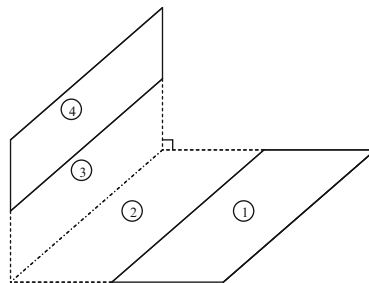
In many cases, it is advantageous to define a single surface (j) as a composite surface consisting of multiple (real or imaginary) surfaces (k), i.e.:

$$A_j = \sum A_k \quad (4.39)$$

For a composite surface j , made up of multiple surfaces k , since view factors are additive:

$$F_{ij} = \sum A_{ik} \quad (4.40)$$

Example 6 For the geometry shown below, use shape factor algebra to develop an expression for the view factor between surface 1 and surface 4 that could be evaluated from the shape factor relations provided in Appendix D.



Solution The desired view factor is F_{14} . For simplicity of nomenclature, denote surface A as a composite surface made up of surfaces 1 and 2. Similarly, denote surface B as a composite surface made up of surfaces 3 and 4. Then, from the additive property of shape factors:

$$A_A F_{AB} = A_1 F_{1B} + A_2 F_{2B}$$

Both F_{AB} and F_{2B} can be calculated from the appropriate shape factor in Appendix D. Note that

$$F_{1B} = F_{13} + F_{14}$$

$$F_{13} = F_{A3} - F_{23}$$

Combining these two equations gives an expression for F_{1B} :

$$F_{1B} = F_{A3} - F_{23} + F_{14}$$

Substituting this expression into the first equation above:

$$\begin{aligned} A_A F_{AB} &= A_1(F_{A3} - F_{23} + F_{14}) + A_2 F_{2B} \\ &= A_1 F_{A3} - A_1 F_{23} + A_1 F_{14} + A_2 F_{2B} \end{aligned}$$

Solving for F_{14} :

$$\begin{aligned} F_{14} &= \frac{1}{A_1}(A_A F_{AB} - A_2 F_{2B} - A_1 F_{A3} + A_1 F_{23}) \\ &= \frac{1}{A_1}(A_A F_{AB} - A_2 F_{2B}) + F_{23} - F_{A3} \end{aligned}$$

Note that all of the view factors in the above example can be evaluated from the shape factor relations provided in Appendix D.

Gray Diffuse Surfaces

For engineering applications, thermal emission from most surfaces is treated as having diffuse directional characteristics independent of wavelength and temperature. Real surfaces exhibit radiation properties that are so complex that information about these property measurements for many common materials is not available. The gray diffuse surface is a useful model that alleviates many of the complexities associated with a detailed radiation analysis, while providing reasonably accurate results in many practical situations. The advantage of diffuse surface analysis is that radiation leaving the surface is independent of the direction of the incoming radiation, which greatly reduces the amount of computation required to solve the governing equations. Discussions for specularly reflecting surfaces and nongray surfaces can be found in the literature [1, 6].

A convenient method to analyze radiative energy exchange in a diffuse gray enclosure relies on the concepts of radiosity and irradiation introduced earlier. The irradiation of surface i (G_i) is the radiative flux reaching the i^{th} surface regardless of its origin:

$$G_i = \sum_j F_{i-j} J_j \quad (4.41)$$

where J_j is the surface radiosity, defined as the total radiative flux leaving the j^{th} surface including both emitted and reflected radiation:

$$J_i = E_i + \rho_i G_i = \varepsilon_i E_{bi} + \rho_i G_i \quad (4.42)$$

The net rate at which radiation leaves surface i is given by

$$\begin{aligned} Q_i &= A_i(J_i - G_i) = A_i(E_i + \rho_i G_i - G_i) \\ &= A_i(E_i - G_i(1 - \rho_i)) \\ &= A_i(E_i - \alpha_i G_i) \end{aligned} \quad (4.43)$$

since, for a diffuse gray opaque surface $\rho_i = 1 - \alpha_i$. It must be emphasized that the radiosity-irradiation formulation is based on the assumption that each surface has uniform radiosity and irradiation (or equivalently, uniform temperature and uniform heat flux). Physically unrealistic calculations can result if each surface does not approximately satisfy this condition. Larger surfaces should be subdivided into smaller surfaces if necessary.

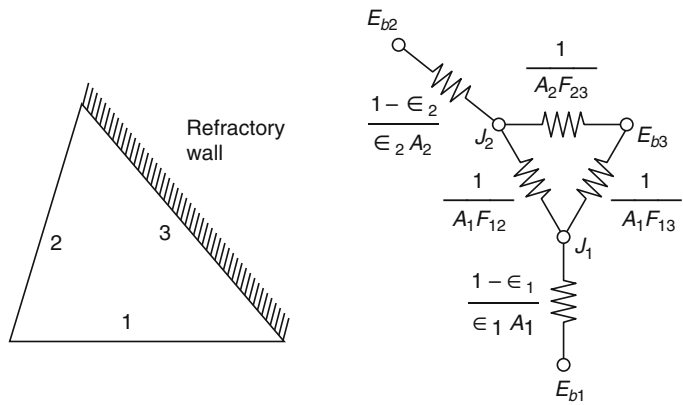
The radiosity-irradiation formulation allows a more physical and graphic interpretation using the resistance network analogy. Eliminating the irradiation G_i from Equations 4.41, 4.42 and 4.43, and substituting $\rho_i = 1 - \varepsilon_i$ gives

$$Q_i = \frac{E_{bi} - J_i}{(1 - \varepsilon_i)/(\varepsilon_i A_i)} = \sum_j \frac{J_i - J_j}{(A_i F_{i-j})^{-1}} \quad (4.44)$$

Note that the second equality in Equation 4.44 can be written as:

$$Q_i = \sum_j A_i F_{i-j} (J_i - J_j) = \sum_j Q_{ij} \quad (4.45)$$

Fig. 4.9 Network analogy for radiative exchange



The denominator in the rightmost term of Equation 4.44 corresponds to resistance in electric circuits. This electrical resistance analogy was first proposed by Oppenheim [20]. As illustrated in Fig. 4.9, the diffuse-gray surface has a radiation potential difference ($E_{bi} - J_i$) and a resistance $(1 - \epsilon_i)/\epsilon_i A_i$. This example also illustrates that an adiabatic surface, such as a reradiating or refractory wall, exhibits a surface temperature that is independent of the surface emissivity or reflectivity.

and scattering within the medium. The intensity, $I_\lambda(S)$, is coupled with the spatial distribution of the extinction coefficient and with temperature through conservation of energy in the medium. The contributions of intensity passing through an area must be integrated over all directions to calculate a net radiative energy flux. The integral nature of radiation makes analysis difficult and simplifications necessary for engineering practice.

Thermal Radiation in Participating Media

The Equation of Transfer

The equation of transfer describes the variation in intensity of a radiant beam at any position along its path in an absorbing-emitting-scattering medium. This equation is the foundation upon which detailed radiation analyses are based, and the source of approximate solutions when simplifying assumptions are made. For a given direction line in the medium, the equation of transfer is

$$\frac{1}{\kappa_\lambda(T, S)} \frac{dI_\lambda(S)}{dS} + I_\lambda(S) = I_{\lambda,b}(T) \quad (4.46)$$

where S represents the physical pathlength and κ_λ represents the spectral extinction coefficient, which includes the effects of both absorption

Spectral Emissivity and Absorptivity

From a microscopic viewpoint, emission and absorption of radiation is attributed to changes in energy levels of atoms and molecules caused by interactions with photons. Tien [21] discusses these effects in gases from an engineering perspective.

Consider a monochromatic beam of radiation passing through a radiating medium of thickness L . For the special case where the temperature and properties of the medium are uniform along this path, the intensity of radiant beam at point x is obtained by integrating Equation 4.46:

$$I_\lambda(x) = I_\lambda(0)\exp(-\kappa_\lambda x) + I_{\lambda,b}(1 - \exp(-\kappa_\lambda x)) \quad (4.47)$$

which accounts for the loss of intensity by absorption and the gain by emission, and where κ_λ denotes the extinction coefficient. The extinction coefficient is generally the sum of two parts:

the absorption coefficient and the scattering coefficient. In many engineering applications, the effects of scattering are negligible and the extinction coefficient represents only absorption. The spectral emissivity for pathlength S in a uniform gas volume can be readily expressed by considering the case of no incident radiation (or $I_\lambda(0) = 0$):

$$\varepsilon_\lambda = \frac{I_\lambda}{I_{\lambda,b}} = 1 - \exp(-\kappa_\lambda S) \quad (4.48)$$

which compares the fraction of energy emitted to the maximum (blackbody) emission at the same temperature for the pathlength S through the material.

The term $\kappa_\lambda S$ in Equation 4.48 is called optical pathlength or opacity and is denoted τ_λ (not to be confused with transmissivity). It can be defined more generally for nonhomogeneous media as:

$$\tau_\lambda = \int_0^S \kappa_\lambda(x) dx \quad (4.49)$$

If $\tau_\lambda \ll 1$, the medium is optically thin at wavelength λ and the properties of the participating medium can generally be approximated as $\varepsilon_\lambda \approx \tau_\lambda$. The medium is considered optically thick when $\tau_\lambda \gg 1$, which implies that the mean penetration distance is much less than the characteristic length of the medium. In optically thick media, as will be described below, the local radiant intensity results only from local emission and the equation of transfer can be approximated by a diffusion equation.

Planck and Rosseland Mean Absorption Coefficients

The mean absorption coefficient is often useful when radiative energy transport theory must be used to describe the local state of a gas at various locations. The mathematical complexity involved in the calculations often dictates a solution based on the gray-gas assumption, where all radiation parameters are considered to be wavelength independent. Thus solutions are given in

terms of mean (gray-gas) absorption coefficients representing average properties over the whole spectrum of wavelengths. The appropriate mean absorption coefficients are the Planck mean, κ_P , for optically thin media, and the Rosseland mean, κ_R , for optically thick media [5, 6, 21].

The Planck mean absorption coefficient is defined as

$$\kappa_P \equiv \frac{\int_0^\infty I_{\lambda,b} \kappa_\lambda d\lambda}{\int_0^\infty I_{\lambda,b} d\lambda} = \frac{\pi}{\sigma T^4} \int_0^\infty I_{b\lambda} \kappa_\lambda d\lambda \quad (4.50)$$

This form of the absorption coefficient is a function of temperature alone and is independent of pressure. The effect of the beam source temperature (e.g., a hot or cold wall) in the gas absorptivity is approximated by a ratio correction [21, 22]

$$\kappa_m = \kappa_P(T_s) \frac{T_s}{T_g} \quad (4.51)$$

where T_s is the source temperature and T_g is the gas temperature. When the Planck mean absorption coefficient is used to estimate the emissivity of a gas, the source temperature is set equal to the gas temperature.

The formulation of radiative transfer is simplified when the medium is optically thick. In this case, the radiative transfer can be regarded as a diffusion process (the Rosseland or diffusion approximation), and the governing equation is approximated by:

$$\begin{aligned} q_r'' &\approx -\frac{4}{3} \frac{1}{\kappa_R} \frac{\partial E_{\lambda,b}}{\partial x} = -\frac{4}{3} \frac{1}{\kappa_R} \frac{\partial (\sigma T^4)}{\partial x} \\ &= -\frac{16\sigma}{3} T^3 \frac{1}{\kappa_R} \frac{\partial T}{\partial x} \end{aligned} \quad (4.52)$$

Evaluation of the total heat flux in an optically thick medium is simplified by defining the Rosseland mean absorption coefficient which is independent of wavelength:

$$\frac{1}{\kappa_R} \equiv \int_0^\infty \frac{1}{\kappa_\lambda} \frac{\partial E_{\lambda,b}}{\partial E_b} d\lambda \quad (4.53)$$

In Equation 4.53, $\partial E_{\lambda,b}/\partial E_b$ is evaluated from the Planck distribution after setting $T = (E_b/\sigma)^{1/4}$. The Rosseland mean absorption coefficient is not well defined for gases under ordinary conditions because astronomically long pathlengths are required to make the windows between the bands optically thick. However, the Rosseland limit is useful when dealing with gases in the presence of soot particles, which are characterized by a continuous spectrum. The source temperature effect is accounted for by using Equation 4.51 in the same manner as for the Planck mean absorption coefficient.

The radiating gas in many actual fire systems is neither optically thin nor optically thick, so it may be necessary to use band theory to rigorously calculate a mean absorption coefficient, κ_m . However, with a reasonable estimate of the mean absorption coefficient, radiative transport calculations are much more convenient.

Mean Beam Length for Homogeneous Gas Bodies

The concept of mean beam length is a powerful and convenient tool to calculate the energy flux from a radiating homogeneous gas volume to its boundary surface. It may also be used to approximate radiative energy flux for a nonhomogeneous gas, especially when more elaborate calculations are not feasible. Consider the coordinate system given in Fig. 4.3, where dA is a differential area on the boundary surface of the gas body. The radiative heat flux from the gas body to dA is

$$\dot{q}_r'' = \int_0^\infty \int_\Omega \varepsilon_\lambda(X) I_{\lambda,b} \cos(\theta) d\lambda d\Omega \quad (4.54)$$

where the spectral emissivity, ε_λ , is a function of pressure pathlength:

$$X \equiv \int_0^S P_a x(\xi) d\xi \quad (4.55)$$

which in turn varies with solid angle Ω according to the gas body geometry. In practical situations, the calculation of \dot{q}_r'' is more convenient in terms of total emissivity, which is often available in chart form. From the definition of total emissivity, Equation 4.54 can be expressed as:

$$\dot{q}_r'' = \frac{\sigma T^4}{\pi} \int_\Omega \varepsilon(X) \cos(\theta) d\Omega \equiv \sigma T^4 \varepsilon(L) \quad (4.56)$$

which gives the definition of mean beam length, L , for a gas body, where $\varepsilon(L)$ has the same functional form as $\varepsilon(X)$. Physically, the mean beam length represents the equivalent radius of a hemispherical gas body such that it radiates a flux to the center of its base equal to the average flux radiated to the boundary surface by the actual volume of gas. The determination of the mean beam length is simplified when the gas is optically thin and only the geometry of the gas body enters the calculation. In the optically thin limit, it is convenient to define

$$L = L_0 \equiv \frac{1}{\pi} \int_\Omega X \cos(\theta) d\Omega \quad (4.57)$$

where L_0 is called the geometric mean beam length. In the optically thick limit, a correction factor (C) can be used to obtain reasonable radiative heat flux estimates:

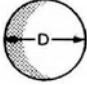
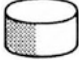



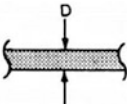
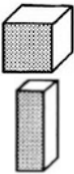
$$L \approx CL_0 \quad (4.58)$$

In Table 4.10, L_0 and C have been provided for a variety of gas body shapes. For an arbitrarily shaped gas volume, the geometric beam length from the gas volume to the entire boundary surface can be estimated by:

$$L_0 = \frac{4V}{A} \quad (4.59)$$

where V and A are the volume and the area of the boundary surface of the gas body, respectively. The correction factor C is approximately 0.9.

Table 4.10 Mean beam lengths for various gas body shapes

Geometry of gas body		Radiating to	Geometric mean beam length L_0	Correction factor C
Sphere		Entire surface	$0.66 D$	0.97
Cylinder $H = 0.5 D$		Plane and surface	$0.48 D$	0.90
		Concave surface	$0.52 D$	0.88
		Entire surface	$0.50 D$	0.90
Cylinder $H = D$		Center of base	$0.77 D$	0.92
		Entire surface	$0.66 D$	0.90
Cylinder $H = 2 D$		Plane end surface	$0.73 D$	0.82
		Concave surface	$0.82 D$	0.93
		Entire surface	$0.80 D$	0.91
Semi-infinite cylinder $H \rightarrow \infty$		Center of base	$1.00 D$	0.90
		Entire base	$0.81 D$	0.80
Infinite slab		Surface element	$2.00 D$	0.90
		Both bounding planes	$2.00 D$	0.90
Cube $D \times D \times 4D$		1×4 face	$0.90 D$	0.91
		1×1 face	$0.86 D$	0.83
		Entire surface	$0.89 D$	0.91

Thermal Radiation Properties of Combustion Products

Radiation Properties of Gases

The emissivity of any gas is a strong function of wavelength, varying by as much as several orders of magnitude over small changes in wavelength. However, the level of accuracy required in engineering calculations, where many of the parameters are difficult to measure or estimate, seldom requires high resolution emissivity spectra. Where wavelength dependence of radiative

heat flux is a concern, gas properties may be calculated using the exponential wide-band model [23]. The uncertainties involved in estimating parameters to calculate radiative heat flux make average properties such as total emissivity a useful tool. The first comprehensive total emissivity charts were formulated by Hottel and coworkers to summarize work performed up to about 1945. Modern formulations for the emissivity of gases have been summarized by Edwards [22].

Total emissivity charts for water vapor and carbon dioxide [22] are provided in Figs. 4.10 and 4.11, respectively. Gas emissivity can be

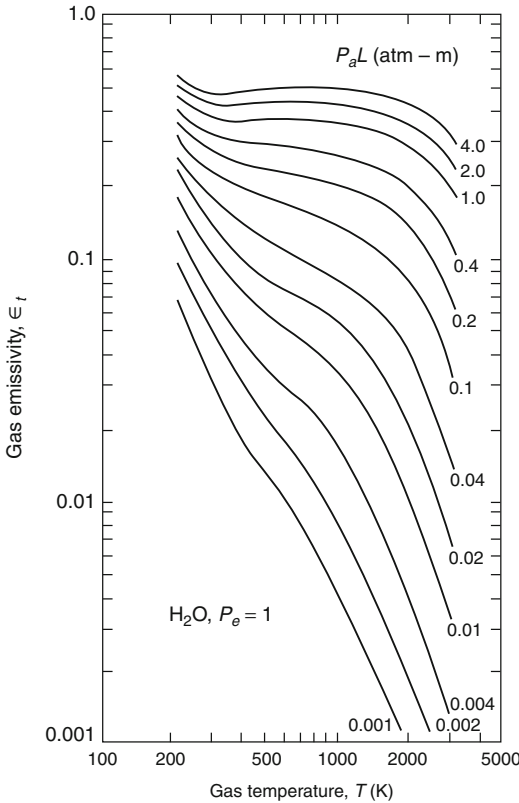


Fig. 4.10 Total emissivity of water vapor

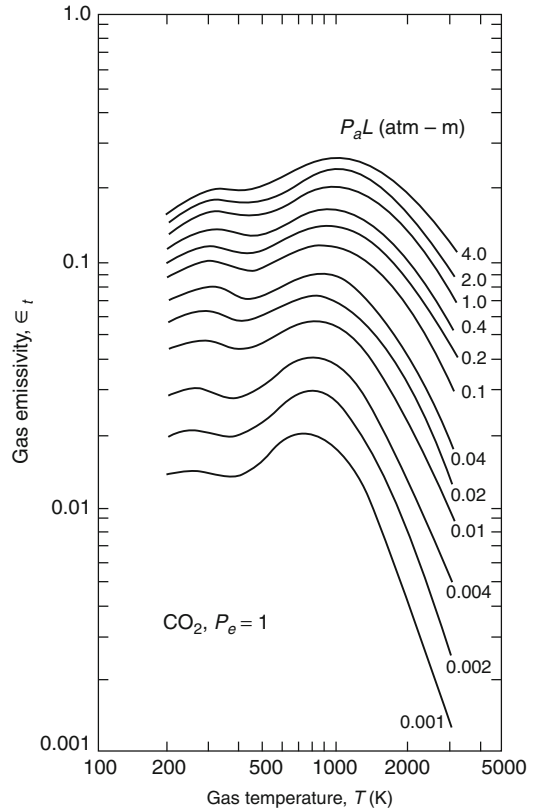


Fig. 4.11 Total emissivity of carbon dioxide

read off these charts from the partial pressure and temperature of each gas and the mean beam length for the gas volume geometry. Correction factors for the chart emissivities are available in the literature for the pressure effect on water vapor emissivity [24], the pressure effect on carbon dioxide emissivity [5, 6], and the band overlap for mixtures of the two gases [25]. For most fire protection engineering applications, the pressure correction factors are 1.0 and the band overlap correction is approximately $\Delta\epsilon \approx \frac{1}{2}\epsilon_{CO_2}$ for medium to large fires. Assuming the carrier gas is transparent (e.g., air), the emissivity is:

$$\epsilon_g = C_{H_2O}\epsilon_{H_2O} + C_{CO_2}\epsilon_{CO_2} - \Delta\epsilon \approx \epsilon_{H_2O} + \frac{1}{2}\epsilon_{CO_2} \quad (4.60)$$

At temperatures below 400 K, the older charts by Hottel [5, 6] may be more reliable than the charts

in Figs. 4.10 and 4.11, and the use of wide-band models is advised to estimate the band overlap correction instead of using the correction charts at these lower temperatures [26]. For crucial engineering decisions, wide-band model block calculations as detailed by Edwards [22] are recommended over the graphical chart method to determine total emissivity.

Other gases such as sulfur dioxide, ammonia, hydrogen chloride, nitric oxide, and methane have been summarized in chart form [5]. The carbon monoxide chart by Hottel is not recommended for use [27] due to uncertainties most likely introduced by traces of carbon dioxide in the original experiments. Spectral and total properties have been published for some of the important hydrocarbon gases, e.g., methane, acetylene, and propylene [28–30]. Mixtures of several hydrocarbon gases are subject to band

overlapping, and appropriate corrections must be made to avoid overestimating total emissivity of a mixture of fuels.

The total emissivity for a gas in the optically thin limit can be calculated from the Planck mean absorption coefficient. Graphs of the Planck mean absorption coefficient for various gases that are important in fires are shown in Fig. 4.12, which can be used with Equation 4.48 to estimate the total emissivity (by assuming that total properties represent a spectral average value).

Radiation Properties of Soot

In a nonhomogeneous (e.g., with soot) medium, scattering becomes an important radiative mechanism in addition to absorption and emission. The absorption and scattering behavior of a single particle can be described by solving the electromagnetic field equations; however, many physical idealizations and mathematical approximations are necessary. The most common assumptions include perfectly spherical particles, uniformly or randomly distributed particles, and

interparticle spacing so large that the radiation for each particle can be treated independently.

Soot particles are produced as a result of incomplete combustion and are usually observed to be in the form of spheres, agglomerated chunks, and long chains. They are generally very small (50–1000 Å where $1 \text{ \AA} = 10^{-10} \text{ m} = 10^{-4} \text{ \mu m}$) compared to infrared wavelengths, so that the Rayleigh limit is applicable to the calculation of radiation properties [31, 32]. Soot particles are normally characterized by their optical properties, size, shape, and chemical composition (hydrogen-carbon ratio). From a heat transfer viewpoint, radiation from a soot cloud is predominantly affected by the particle size distribution and can be considered independent of the chemical composition [31]. Soot optical properties are relatively insensitive to temperature changes at elevated temperatures, but as shown in Fig. 4.13, room temperature values representative of soot in smoke do show appreciable deviations.

By choosing appropriate values of optical constants for soot, the solution for the electromagnetic field equations gives [33]

Fig. 4.12 Planck mean absorption coefficient for various gases

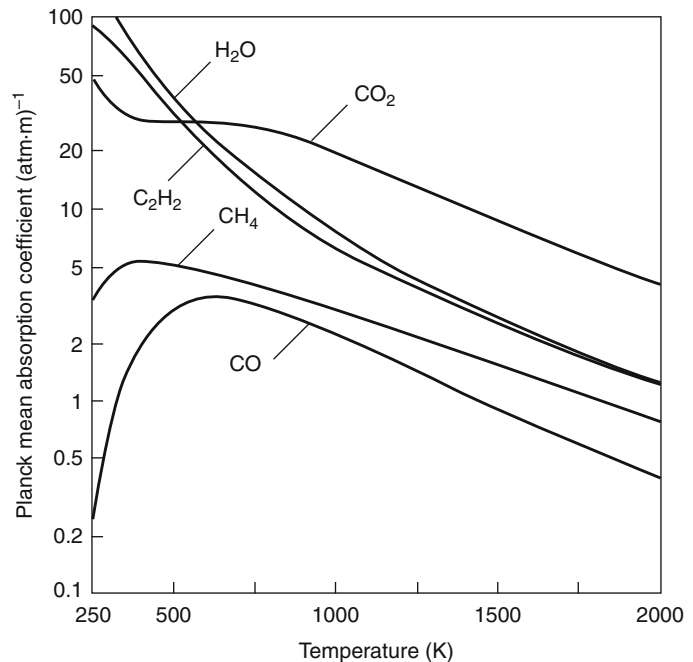
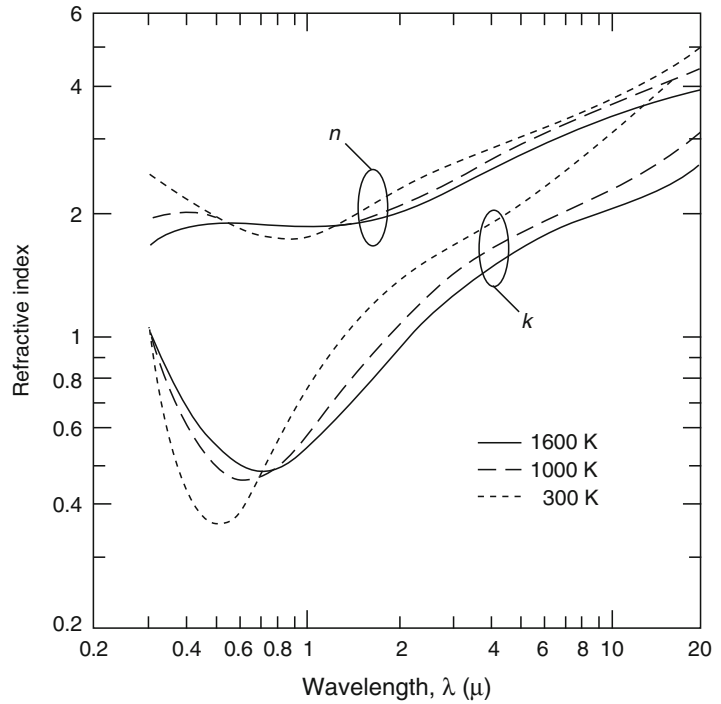


Fig. 4.13 Optical constants for soot



$$k_{\lambda} = \frac{C_0}{\lambda} f_v \quad (4.61)$$

where f_v is the soot volume fraction (generally about 10^{-6} in flames) and C_0 , a constant between 2 and 6 dependent on the complex index of refraction $m = n - ik$, is given by

$$C_0 = \frac{36\pi nk}{(n^2 - k^2 + 2)^2 + 4n^2k^2} \quad (4.62)$$

Equations 4.61 and 4.62 can be used to evaluate the Planck mean absorption coefficient in the optically thin limit [34], giving:

$$\kappa_P = 3.83 \frac{C_0}{C_2} f_v T \quad (4.63)$$

where C_2 is Planck's second constant (1.4388×10^{-2} m-K). The Rosseland mean absorption coefficient in the optically thick limit is

$$\kappa_R = 3.6 \frac{C_0}{C_2} f_v T \quad (4.64)$$

A mean coefficient that may be used for the entire range of optical thickness is suggested as

$$\kappa_R = 3.72 \frac{C_0}{C_2} f_v T \quad (4.65)$$

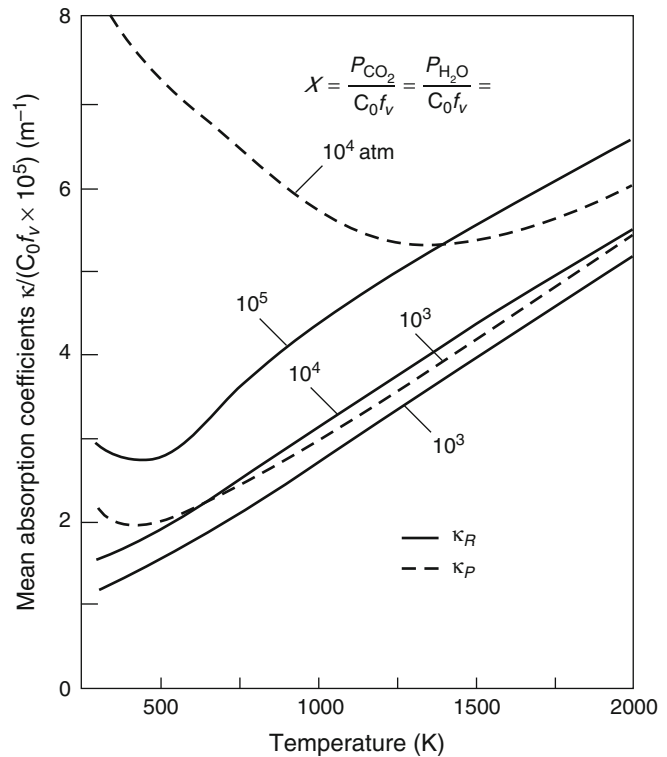
to be used in Equation 4.66 for the soot radiation calculations. Typical temperatures, volume fractions, and mean absorption coefficients for soot particles in the luminous flames of various fuels are tabulated in Table 4.11.

Radiation Properties of Gas-Soot Mixtures

The calculation of the total emissivity of a gas-soot mixture requires information on basic flame parameters such as soot volume fraction, soot absorption coefficient, temperature and geometric length of the flame, and partial pressure of the participating gas components [35]. These parameters can be estimated for various types of

Table 4.11 Radiative properties for soot particles

	Fuel, composition	κ_S (m^{-1})	$f_v \times 10^6$	$T_s(K)$
Gas fuels	Methane, CH ₄	6.45	4.49	1289
	Ethane, C ₂ H ₆	6.39	3.30	1590
	Propane, C ₂ H ₈	13.32	7.09	1561
	Isobutane, (CH ₃) ₃ CH	16.81	9.17	1554
	Ethylene, C ₂ H ₄	11.92	5.55	1722
	Propylene, C ₃ H ₆	24.07	13.6	1490
	n-butane, (CH ₃)(CH ₂) ₂ (CH ₃)	12.59	6.41	1612
	Isobutylene, (CH ₃) ₂ CCH ₂	30.72	18.7	1409
	1,3-butadiene, CH ₂ CHCHCH ₂	45.42	29.5	1348
Solid Fuels	Wood, \approx (CH ₂ O) _n	0.8	0.362	1732
	Plexiglas, (C ₅ H ₈ O ₂) _n	0.5	0.272	1538
	Polystyrene, (C ₈ H ₈) _n	1.2	0.674	1486

Fig. 4.14 Mean absorption coefficients for luminous flames and smoke

fuel when actual measurements are unavailable for a particular situation. The following equation is a good approximation [36] for total emissivity of homogeneous gas-soot mixtures:

$$\epsilon_t = (1 - \exp(-\kappa S)) + \epsilon_g \exp(-\kappa_s S) \quad (4.66)$$

where S is the physical pathlength, ϵ_g is the total emissivity of the gas alone, and κ_s is the effective absorption coefficient of the soot. The Planck mean absorption coefficients for gas-soot mixtures in luminous flames and smoke are shown in Fig. 4.14.

Application to Flame and Fire

Heat Flux Calculation from a Flame

Prediction of the radiative heat flux from a flame is important in determining ignition and fire spread hazard, and in the development of fire detection devices. The shape of flames under actual conditions is transient, which makes detailed radiation analysis cumbersome. In most calculations, flames are idealized as simple geometric shapes such as plane layers or axisymmetric cylinders and cones. A cylindrical geometry, shown in Fig. 4.15, will be analyzed here and used in a sample calculation.

Assuming κ_λ is independent of pathlength, integration of the transport equation (Equation 4.48) yields [37]

$$I_\lambda = I_{b\lambda} \left(1 - \exp \left(\frac{-2\kappa_\lambda}{\sin(\theta)} \sqrt{r^2 - L^2 \cos^2(\phi)} \right) \right) \quad (4.67)$$

where θ , ϕ , r , and L are geometric variables defined in Fig. 4.15. The monochromatic radiative heat flux on the target element is given by

$$\frac{d\dot{q}_r''}{d\lambda} = \int_{\Omega} \frac{I_\lambda}{|\vec{R}|} (\vec{n} \cdot \vec{R}) d\Omega \quad (4.68)$$

Where \vec{n} is a unit vector normal to the target element dA and \vec{R} is the line-of-sight vector extending between dA and the far side of the flame cylinder. Evaluation of Equation 4.68 is quite lengthy, but under the condition of $L/r \geq 3$, it can be simplified to [37]

$$\frac{d\dot{q}_r''}{d\lambda} = \pi I_{\lambda,b} \epsilon_\lambda (F_1 + F_2 + F_3) \quad (4.69)$$

where the shape factor constants and emittance are defined as

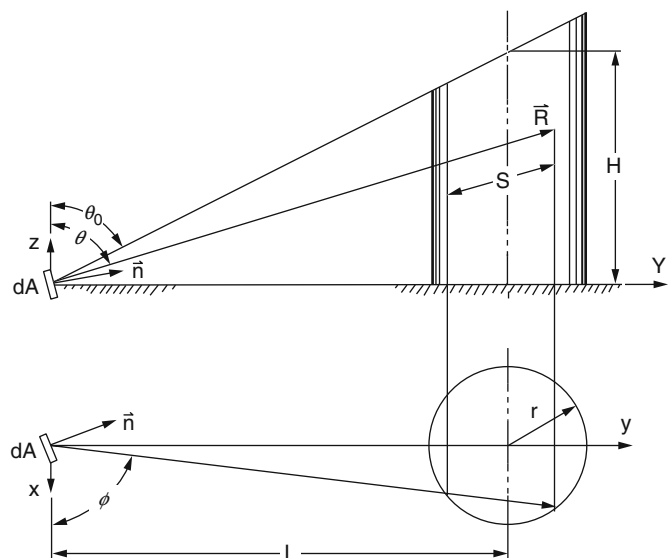
$$F_1 = \frac{u}{4\pi} \left(\frac{r}{L} \right)^2 (\pi - 2\theta_0 + \sin(2\theta_0)) \quad (4.70a)$$

$$F_2 = \frac{v}{4\pi} \left(\frac{r}{L} \right) (\pi - 2\theta_0 + \sin(2\theta_0)) \quad (4.70b)$$

$$F_3 = \frac{w}{\pi} \left(\frac{r}{L} \right) \cos^2(\theta_0) \quad (4.70c)$$

$$\epsilon_\lambda = 1 - \exp(-0.7\mu_\lambda) \quad (4.71)$$

Fig. 4.15 Schematic of a cylindrical flame



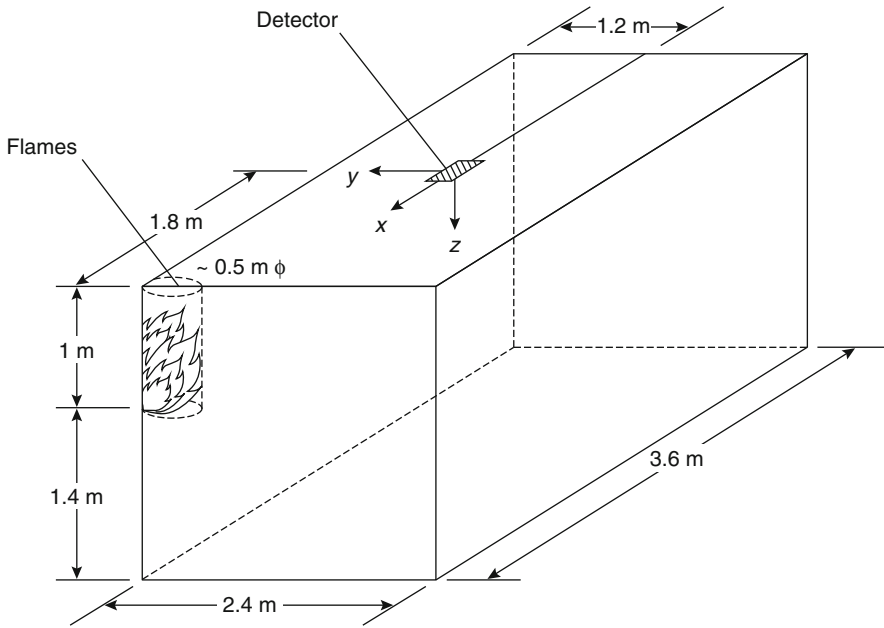


Fig. 4.16 Example calculation for flux to target element from flame

The parameters in the definitions are given by

$$\theta_0 = \tan^{-1}(L/H) \tag{4.72a}$$

$$\mu_\lambda = 2r \frac{\kappa_\lambda}{\sin\left(\frac{\theta_0}{2} + \frac{\pi}{4}\right)} \tag{4.72b}$$

$$\vec{n} = u\vec{i} + v\vec{j} + w\vec{k} \tag{4.72c}$$

If the flame is considered to be homogeneous and Equation 4.69 is integrated over all wavelengths, the total heat flux is:

$$\dot{q}_r'' = \varepsilon_m E_b \sum_{j=1}^3 F_j \tag{4.73}$$

Example 7 As shown in Fig. 4.16, a fire detector is located at the center of the ceiling in a room (2.4 × 3.6 × 2.4 m) with wood wall linings. The sprinkler system is capable of extinguishing fires smaller than 0.5 m in diameter × 1.0 m high. For this example, determine the appropriate heat flux setting for the detector, using a worst case scenario of ignition in one of the upper ceiling corners.

Solution First, the condition of $L/r \geq 3$ should be checked to verify that the previous analysis is applicable.

$$\frac{L}{r} \approx \frac{\sqrt{1.2^2 + 1.8^2}}{0.25} = 8.65 > 3 \tag{4.74}$$

The unit normal vector to the detector is given by $\vec{n} = \vec{k}$, the polar angle $\theta_0 = \tan^{-1}(1.8/1.2) = 1.068$ is determined from Equation 4.72a, and the shape factors are evaluated from Equations 4.70a, 4.70b, and 4.70c:

$$F_1 = 0 \tag{4.75a}$$

$$F_2 = 0 \tag{4.75b}$$

$$F_3 = \frac{1}{\pi} \left(\frac{0.25}{1.818} \right) \cos^2(1.068) = 0.0102 \tag{4.75c}$$

From Equation 4.73, the radiant heat flux can be calculated as:

$$\begin{aligned} \dot{q}_r'' &= (1 - \exp(-\kappa_m S)) \sigma T_f^4 F_3 \\ &= (1 - \exp(-0.8 \times 0.5)) \times 5.67 \times 10^{-8} \times 1732^4 \times 0.0102 \\ &= 1.7 \text{ kW/m}^2 \end{aligned} \tag{4.76}$$

where wood flame properties were taken from Table 4.11. If the geometry of the example had been $L/r < 3$, it would have been necessary to interpolate between the $L/r = 3$ case and the $L/r = 0$ case, which has been obtained accurately [6, 37]. If the detector is pointed directly at the burning corner in this example (i.e., $\vec{n} = 0.55 \vec{i} + 0.83 \vec{j}$), the calculated heat flux jumps to 9.0 kW/m^2 , showing the strong influence of direction in calculations of radiation heat transfer.

Hot upper gas layers are composed of strongly participating media such as carbon dioxide, water vapor, and soot particles. Heat flux from the smoke layer is directly related to ignition of remote surface locations such as furniture or floor carpets. The schematic in Fig. 4.17 will be considered in a radiative transport analysis and example calculation. The calculation is based on a considerably simplified formulation which provides reasonable results with only a small penalty in accuracy.

Integration of Equation 4.46 over the pathlength S through the smoke layer yields

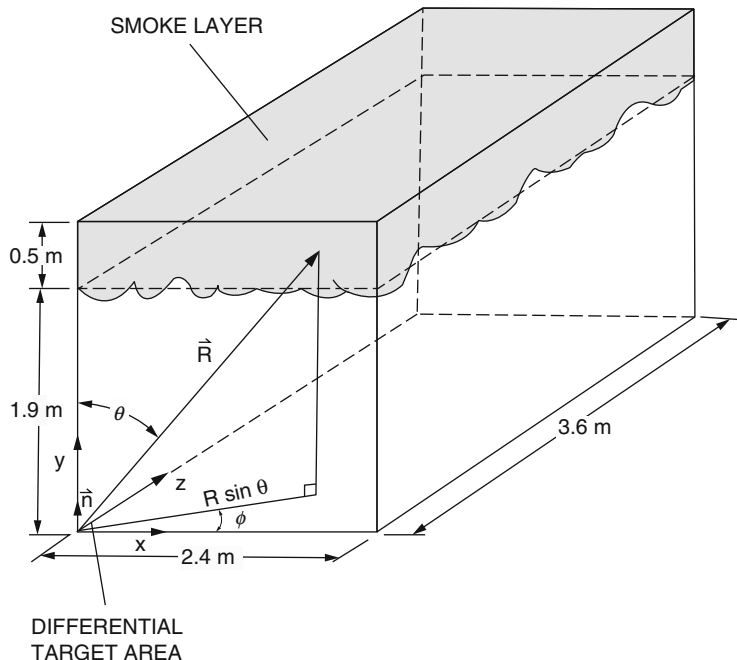
$$I(S) = \frac{\sigma T^4}{\pi} \left(1 - \left(\frac{T_w}{T} \right)^4 \right) \exp(-\kappa S) \tag{4.77}$$

Heat Flux Calculation from a Smoke Layer

Consider the situation shown below in Fig. 4.17 involving radiative heat transfer in a compartment fire with a hot gas layer located below the ceiling.

The monochromatic radiative heat flux on a differential target element is again given by Equation 4.68. However, for the present geometry of

Fig. 4.17 Example calculation for flux to target element from smoke layer



the ceiling layer and enclosure surface, integration of Equation 4.68 is quite time-consuming since the upper and lower bounds of the integral vary with the angle of the pathlength. The calculation can be simplified by assuming as a first order approximation that the lower face of the smoke layer is an isothermal surface. Using this assumption, the problem can be handled using the simple relations of radiative exchange in a nonparticipating medium between gray surfaces (the absorption of the clear air below the smoke layer is negligible). The radiosity and irradiation of each surface in the enclosure is:

$$J_i = \varepsilon_i \sigma T_i^4 + (1 - \varepsilon_i) G_i \quad (4.78a)$$

$$G_i = \sum_j F_{i-j} J_j \quad (4.78b)$$

After solving the simultaneous equations for all J_i and G_i , the net heat flux on any of the surfaces can be calculated from

$$\dot{q}_{r,i}'' = J_i - G_i \quad (4.79)$$

This situation is considered in Example 8 below.

Example 8 A smoke layer 0.5 m thick is floating near the ceiling of a room with dimensions of $3.6 \times 2.4 \times 2.4$ m. (See Fig. 4.17.) The floor is made from wood (emissivity = 0.9), and the four side walls are painted concrete (emissivity = 0.94). The calculation will determine the heat flux in a bottom corner of the room, assuming that each surface in the enclosure is kept at constant temperature: the smoke layer at 1400 K, the side walls at 800 K, and the floor at 300 K. Assume there is a differential target area 0.01 m^2 in one of the corners of the floor, and also at the floor temperature of 300 K.

Solution The bottom of the smoke layer will be designated surface 1, the floor will be surface 2, and the differential target area in the bottom corner will be surface 3. Only four surfaces are required since the four side walls can be treated as a single surface 4. Shape factors F_{12} and F_{31} can be found in Appendix D, and from these two

factors, the remaining shape factors are determined by shape factor algebra:

$$F_{12} = 0.3242$$

$$F_{31} = 0.1831$$

$$F_{13} = \frac{A_3}{A_1} F_{31} = 0.0002$$

$$F_{14} = 1 - F_{12} - F_{13} = 0.6756$$

Continuing in a similar fashion, the other shape factors are obtained as:

$$F_{21} = 0.3242 \quad F_{31} = 0.1831 \quad F_{41} = 0.2560$$

$$F_{22} = 0.0000 \quad F_{32} = 0.0000 \quad F_{42} = 0.2561$$

$$F_{23} = 0.0000 \quad F_{33} = 0.0000 \quad F_{43} = 0.0003$$

$$F_{24} = 0.6758 \quad F_{34} = 0.8169 \quad F_{44} = 0.4876$$

The emissivity for the smoke layer can be estimated from the mean absorption coefficient for a wood flame (Table 4.11) as:

$$\begin{aligned} \varepsilon_1 &= 1 - \exp(-\kappa_m S) = 1 - \exp(-0.8 \times 0.5) \\ &= 0.33 \end{aligned}$$

The blackbody emissive power of each surface is calculated as σT^4 , for example:

$$\begin{aligned} (\sigma T^4)_1 &= 5.6696 \times 10^{-8} \times 1400^4 \\ &= 217.8 \text{ kW/m}^2 \end{aligned}$$

From Equations 4.78a and 4.78b, the radiative fluxes to and from each surface are determined by solving the eight simultaneous equations:

$$J_1 = 88.7 \text{ kW/m}^2 \quad G_1 = 17.7 \text{ kW/m}^2$$

$$J_2 = 4.7 \text{ kW/m}^2 \quad G_2 = 43.3 \text{ kW/m}^2$$

$$J_3 = 3.9 \text{ kW/m}^2 \quad G_3 = 34.8 \text{ kW/m}^2$$

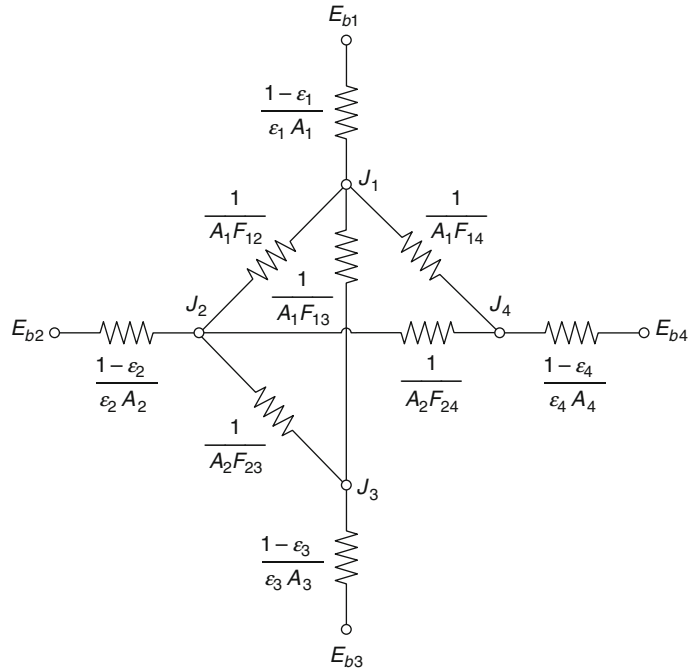
$$J_4 = 23.9 \text{ kW/m}^2 \quad G_4 = 34.3 \text{ kW/m}^2$$

The net radiative heat flux on the target element from Equation 4.79 is

$$\dot{q}_{r,3}'' = J_3 - G_3 = -30.9 \text{ kW/m}^2$$

where the negative sign indicates that heat must be removed from the target element so it remains

Fig. 4.18 Equivalent resistance network for an enclosure



in equilibrium. This example also could have been solved by the resistance network method shown in Fig. 4.18)

- $I_{\vec{i}, \vec{j}, \vec{k}}$ Radiation intensity (W/m^2)
- $\vec{i}, \vec{j}, \vec{k}$ Cartesian coordinate direction vectors
- J Radiosity or radiative heat flux leaving surface (W/m^2)
- k Boltzmann constant ($1.3806 \times 10^{-23} \text{ J/K}$), or infrared optical constant of soot (imaginary component), or thermal conductivity (W/m K)
- L Mean beam length or distance (m)
- L_0 Geometrical mean beam length (m)
- n Index of refraction (c_0/c) or infrared optical constant of soot (real component)
- \vec{n} Unit normal vector
- P_a Partial pressure of absorbing gas (Pa)
- P_e Effective pressure (Pa)
- Q Energy rate (W)
- q'' Heat flux (W/m^2)
- \vec{R} Line of sight vector
- r Radius of cylinder (m)
- S Pathlength (m)
- T Temperature (K)
- t Time (s)
- u, v, w Cartesian components of unit vector \vec{n}
- V Volume (m^3)

Nomenclature

- A Area (m^2)
- C Correction factor for mean beam length
- C_0 Soot concentration parameter
- C_2 Planck's second constant ($1.4388 \times 10^{-2} \text{ m} \cdot \text{K}$)
- c Speed of light in the medium (m/s)
- c_0 Speed of light in a vacuum ($2.998 \times 10^8 \text{ m/s}$)
- E Radiative emissive power (W/m^2)
- F_{i-j} Configuration factor from surface i to surface j
- f_v Soot volume fraction
- G Irradiation or radiative heat flux received by surface (W/m^2)
- H Height (m)
- h Planck's constant ($6.6256 \times 10^{-34} \text{ J s}$)

X	Pressure pathlength, $\int_0^s P_a x(\xi) d(\xi)$ (atm-m)
x	Spatial coordinate (m)

Greek Symbols

α	Absorptivity or thermal diffusivity $k/\rho c_p$ (m^2/s)
β	Angle from normal (radians)
ϵ	Emissivity
θ	Polar angle (radians)
κ	Extinction coefficient or absorption coefficient (m ⁻¹)
λ	Wavelength (m)
μ	Micron (10^{-6} m)
μ_λ	Defined parameter, Equation 4.73
ν	Frequency (s^{-1})
ξ	Integration dummy variable
ρ	Reflectivity or density (kg/m^3)
Ω	Solid angle (steradians)
σ	Stefan-Boltzmann constant ($5.6696 \times 10^{-8} W/m^2K^4$)
τ	Transmissivity or optical pathlength
ϕ	Azimuthal angle (radians)
χ	Fractional measure

Subscripts

a	Actual
b	Blackbody or base
e	External
f	Flame
g	Gas
i	Initial or i^{th} surface
j	Summation variable or j^{th} surface
m	Mean value
0	Original
P	Planck mean
R	Roseland mean
s	Surface or soot
t	Total
w	Wall
λ	Spectral wavelength
ν	Spectral frequency
∞	Ambient

References

1. J. deRis, *17th Symposium (International) on Combustion*, 1003, Combustion Institute, Pittsburgh, PA (1979).
2. S.C. Lee and C.L. Tien, *Progress in Energy and Combustion Science*, 8, 41 (1982).
3. G.M. Faeth, S.M. Jeng, and J. Gore, in *Heat Transfer in Fire and Combustion Systems*, American Society of Mechanical Engineers, New York (1985).
4. Incropera, F.P. and DeWitt, D.P., *Fundamentals of Heat and Mass Transfer*, John Wiley & Sons, New York, 2002.
5. H.C. Hottel and A.F. Sarofim, *Radiative Heat Transfer*, McGraw-Hill, New York (1967).
6. R. Siegel and H.R. Howell, *Thermal Radiation Heat Transfer*, McGraw-Hill, New York (1981).
7. Bejan, A., *Heat Transfer*, John Wiley & Sons, New York, 1993.
8. Hallman, J.R., "Ignition characteristics of plastics and rubber," Ph.D. Dissertation, University of Oklahoma, 1971.
9. Hallman, J.R., Welker, J.R., and Sliepcevich, C.M., "Polymer surface reflectance-absorptance characteristics," *Polymer Engineering and Science* 14: 717-723 (1974).
10. Hallman, J.R., Sliepcevich, C.M., and Walker, J.R., "Radiation absorption for polymers: The radiant panel and carbon arcs as radiant heat sources," *Journal of Fire & Flammability* 9: 353-366 (1978).
11. Wesson, H.R., Welker, J.R., and Sliepcevich, C.M., "The piloted ignition of wood by thermal radiation," *Combustion and Flame* 16: 303-310 (1971).
12. Försth, M. and Roos, A., "Absorptivity and its Dependence on Heat Source Temperature and Degree of Thermal Breakdown," *Fire and Materials* 35: 285-301 (2011).
13. Janssens, M., "Piloted ignition of wood: a review," *Fire and Materials* 15: 151-167 (1991).
14. Janssens, M. and Douglas, B., "Wood and wood products," in *Handbook of Building Materials for Fire Protection*, Ed. Harper, C.A., pp. 7.1-7.58, McGraw-Hill, New York, 2004.
15. Kashiwagi, T. and Ohlemiller, T.J., "A study of oxygen effects on nonflaming transient gasification of PMMA and PE during thermal irradiation," *Proceedings of the Combustion Institute* 19: 815-823 (1982).
16. Modak, A.T. and Croce, P.A., "Plastic pool fires," *Combustion and Flame* 30: 251-265 (1977).
17. E.M. Sparrow and R.D. Cess, *Radiation Heat Transfer*, McGraw-Hill, New York (1978).
18. J.R. Howell, *A Catalog of Radiation Configuration Factors*, McGraw-Hill, New York (1982).
19. C.L. Tien, in *Handbook of Heat Transfer Fundamentals*, McGraw-Hill, pp 14.36, New York (1985).

20. Oppenheim, A.K, *Trans. ASME*, **65**, 725, 1956.
21. C.L. Tien, *Advances in Heat Transfer*, **5**, 253 (1968).
22. D.K. Edwards, in *Handbook of Heat Transfer Fundamentals*, McGraw-Hill, pp 14.53, New York (1985).
23. D.K. Edwards, *Advances in Heat Transfer*, **12**, 115 (1976).
24. G.B. Ludwig, W. Malkmus, J.E. Reardon, and J.A.L. Thompson, *Handbook of Radiation from Combustion Gases*, NASA SP- 3080, Washington (1973).
25. T.F. Smith, Z.F. Shen, and J.N. Friedman, *Journal of Heat Transfer*, **104**, 602 (1982).
26. J.D. Felske and C.L. Tien, *Combustion Science and Technology*, **11**, 111 (1975).
27. M.M. Abu-Romia and C.L. Tien., *Journal of Quantitative Spectroscopy and Radiative Transfer*, **107**, 143 (1966).
28. M.A. Brosmer and C.L. Tien, *Journal of Quantitative Spectroscopy and Radiative Transfer*, **33**, 521 (1985).
29. M.A. Brosmer and C.L. Tien, *Journal of Heat Transfer*, **107**, 943 (1985).
30. M.A. Brosmer and C.L. Tien, *Combustion Science and Technology*, **48**, 163 (1986).
31. S.C. Lee and C.L. Tien, 18th Symposium (International) on Combustion, Combustion Institute, 1159, Pittsburgh (1981).
32. C.L. Tien, in *Handbook of Heat Transfer Fundamentals*, McGraw-Hill, pp 14.83, New York (1985).
33. G.L. Hubbard and C.L. Tien, *Journal of Heat Transfer*, **100**, 235 (1978).
34. J.D. Felske and C.L. Tien, *Journal of Heat Transfer*, **99**, 458 (1977).
35. J.D. Felske and C.L. Tien, *Combustion Science and Technology*, **7**, 25 (1977).
36. W.W. Yuen and C.L. Tien, *16th Symposium (International) on Combustion*, Combustion Institute, 1481, Pittsburgh (1977).
37. A. Dayan and C.L. Tien, *Combustion Science and Technology*, **9**, 41 (1974).

Chris Lautenberger is a fire protection engineer at Reax Engineering Inc. in Berkeley, CA. He is also an Instructor in Cal Poly's Fire Protection Engineering program where he co-teaches courses on Fire Modeling and Fire Dynamics.